HHS Public Access

Author manuscript

Neuron. Author manuscript; available in PMC 2019 December 19.

Published in final edited form as:

Neuron. 2018 December 19; 100(6): 1474–1490.e4. doi:10.1016/j.neuron.2018.10.027.

A brain module for scalable control of complex, multi-motor threat displays

Brian J. Duistermars[1], **Barret D. Pfeiffer**[2], **Eric D. Hoopfer**[1], and **David J. Anderson**[1,2,3,4,5]

[1]Division of Biology and Biological Engineering 156-29, California Institute of Technology, Pasadena, CA 91125, USA

[2]Howard Hughes Medical Institute, California Institute of Technology, Pasadena, CA 91125, USA

[3]Tianqiao and Chrissy Chen Institute for Neuroscience, California Institute of Technology, Pasadena, CA 91125, USA

[4]Lead contact

Summary

Threat displays are a universal feature of agonistic interactions. Whether threats are part of a continuum of aggressive behaviors, or separately controlled, remains unclear. We analyze threats in *Drosophila* and show they are triggered by male cues and visual motion, and comprised of multiple motor elements that can be flexibly combined. We isolate a cluster of ~3 neurons whose activity is necessary for threat displays but not for other aggressive behaviors, and whose artificial activation suffices to evoke naturalistic threats in solitary flies, suggesting that the neural control of threats is modular with respect to other aggressive behaviors. Artificially evoked threats suffice to repel opponents from a resource, in the absence of contact aggression. Depending on its level of artificial activation, this neural threat module can evoke different motor elements in a threshold-dependent manner. Such scalable modules may represent fundamental “building blocks” of neural circuits that mediate complex multi-motor behaviors.

Abstract

Duistermars et al. characterize threat displays in flies, the sensory cues required for this behavior, and identify a compact neural module that controls flexible threat behavior according to its level of activity

[5] Author for correspondence: wuwei@caltech.edu.

Author Contributions

D.J.A. and B.J.D. conceived the project, designed experiments and interpreted the results. B.J.D conducted experiments, made figures, and co-wrote the manuscript with D.J.A. B.D.P. provided reagents and expertise, E.H. originally identified and provided advanced access to R20E08 and Split Gal4s.

Declaration of Interests

The authors declare no competing interests.

Keywords

Animal; aggression; threat; display; scalable; sensory; motor; module; function; territoriality

Introduction

Animals express a repertoire of species-typical, innate social behaviors that are comprised of complex and functionally relevant movements (Craig, 1917; Heinroth, 1911; Whitman, 1919). Despite much recent progress in understanding neural circuits that underlie social behaviors (Chen and Hong, 2018; Emmons, 2018; Hashikawa et al., 2016; Yamamoto and Koganezawa, 2013; Yang and Shah, 2016), the neural mechanisms that coordinate diverse movements into coherent and functionally adaptive social activities are poorly understood. For example, aggression, a prototypic social activity, involves several different kinds of actions, including threat displays, chasing, and attack, that are often expressed in an escalating continuum (Anderson and Perona, 2014; Lorenz, 1970; Miczek et al., 2007). Each of these behaviors is in turn comprised of multiple motor elements. It remains unclear how these different actions and their constituent motor elements are controlled and coordinated. To address this issue, we have investigated the neural control of agonistic threat display.

Threat displays are elicited in conflict situations and often signal intent to escalate from non-contact to contact-mediated agonistic behavior. Threats have adaptive value, in that if they prevent such escalation, they reduce energy expenditure and lower the risk of injury (Blurton Jones, 1968; Lange and Leimar, 2003; Moynihan, 1955). While threat displays are recognizably distinct from other forms of aggression, to a human observer, it is not clear whether they are controlled at the circuit level as part of a continuum of agonistic behaviors, or rather by a distinct and dissociable module or pathway.

Threat displays often involve multiple, characteristic motor elements including size inflation, charging, orientation, and vocalizations (Dierick, 2007; Hurd and Enquist, 2001). For instance, frillneck lizards slash their tails, erect their frills, wave their forelimbs, and bob their heads (Shine, 2008). Nuthatches fan their tail, raise their bills, rapidly extend their wings, and oscillate their bodies side to side (Long, 1982). Gorillas charge forward, swat the ground, beat their chests, and utter barking roars (Emlen, 1962). Threats are thus coordinated but flexible, multi-motor displays, which vary in their intensity and complexity (Darwin, 1873; Hurd and Enquist, 2001; Miczek et al., 2007). How does the brain coordinate multiple motor elements into a coherent, functionally meaningful behavioral display, while affording flexibility in the way those elements are combined?

Here we have investigated the neural control of threats in the vinegar fly, *Drosophila melanogaster* (Chen et al., 2002; Dow and von Schilcher, 1975; Jacobs, 1960). Using automated behavior classification we find that fly threats require both chemosensory cues and visual motion for their elicitation, and are comprised of distinct motor elements whose combinatorial expression varies in complexity and intensity. We isolate a sparse cluster of central brain neurons that, when activated, induce naturalistic threat displays but no other agonistic behaviors. Conversely, silencing these neurons during natural agonistic interactions specifically eliminates threats, but not other aggressive actions. The ability to cleanly

uncouple threats from other forms of aggression suggests that they are controlled via a specific neural module, rather than by a circuit that governs a continuum of agonistic behaviors. We further exploit this modularity to demonstrate that threats indeed function to repel opponents from valuable territories.

Interestingly, we find that different levels of artificial threat module activation can qualitatively and quantitatively substitute for chemosensory or visual motion cues, and can also evoke different motor elements of threat displays in a scalable (variable intensity and complexity), threshold-dependent manner. This scalable control appears to mimic the variable expression of natural threat displays. Together, these data identify a compact neural threat module that may serve to integrate and transform multi-sensory input into flexible motor output, in a manner that varies with its level of activity. Such scalable modules may be fundamental components of the neural systems underlying complex animal behaviors.

Results

Natural threat displays are comprised of distinct motor elements

A quantitative description of a given behavior is a prerequisite for understanding how the nervous system controls that behavior (Krakauer et al., 2017). To rigorously characterize fly threats, we placed two aggressive, single-housed (SH), wild-type (WT) males in a chamber with food (Fig. S1A; Hoyer et al., 2008; Wang et al., 2008), and recorded video of their interactions. We then automatically tracked movement features (Asahina et al., 2014) and trained a supervised classifier (JAABA; Kabra et al., 2012) to identify instances of threats. After screening predicted threats (see Methods), we obtained 465 episodes (N=23 fly pairs) for further analysis. An illustrative example revealed that threateners charge toward the target fly, extend and elevate their wings, and track the target around the arena before dropping their wings and returning to the food (Figs. 1Ai, ii, movie S1).

We measured three parameters to describe the major motor elements of threats (Fig. 1Bi): wing elevation (wing angle, WA); charges (spikes in forward velocity, V); and rapid orientation, or turns (spikes in angular velocity; AV). We defined threat “bouts” as periods when both wings were quickly extended horizontally to an average WA of ~90° each (“pump”), or elevated to the more common wing position, 45° (Figs. 1Bi, S1Bi). Such bouts varied continuously in duration (Fig. S1Bii). In some cases, threateners iterated 4–6Hz spikes in V before and during a bout (~16%, Figs. 1Bii, arrow, S1Ci, orange). This motor pattern was apparent in individual and mean velocity traces (Fig. S1Cii) but not in target velocity (Fig. S1Ci, gray), suggesting it is intrinsically generated. Threateners also iterated AV spikes (Figs. 1Biii, S1Di, black line) that were either turns toward stationary targets (Fig. S1Dii, orange, 14%), turns toward moving targets (black, 73%), or turns away from targets (red, 13%). Finally, although pumps, charges, and turns occurred together at the start of a bout (Fig. 1C, t=0), we observed variable numbers and combinations of motor elements displayed before, during, and after each “threat” (bout ±0.5s, see Methods, Fig. S1E).

To assess the degree to which these clearly distinguishable motor elements occur independently or in combination, we set thresholds in WA, V and AV (Fig. 1B, dashed horizontal lines; see Methods) to binarize instances of elemental wing pumps, wing

elevations, charges, turns, and periods of immobility (Fig. 1D). We next analyzed the frequency of all possible element singlets, doublets, and triplets in “element space” for all threats (Fig. 1Ei). This analysis indicated that some elements and element combinations were more prevalent, while others were rare (Fig. 1Eii). It is possible that more fine-grained kinematic analysis would reveal additional element combinations. From these data, we generated a motor element space transition matrix (Fig. S1F) and corresponding transition diagram (Fig. 1F). Nodes in the diagram are arranged in 2D for compactness and to minimize distance between transitional partners (exclusions indicated, Fig. 1Eiii).

Several generalizations can be extracted from this diagram (Fig. 1F), which we describe in terms of rows from bottom to top. First, periods of row 1 immobility (node 6) occurred intermittently, between charges and turns and before, during, and after a bout (Fig. 1D, bottom raster). In row 2, flies executed charges (4), turns (5), or both (13, Figs. 1Bii, arrow, S1C, D). In row 3, charges (10) and turns (11) were combined with wing elevation (15, Fig. 1Bi). Flies then transitioned either to row 4 immobility with wings elevated (12) or to row 5 pumps with charges and turns (14, Fig. 1Bi). Charges, turns, and immobility thus occurred independently or in combination with wing elevation, while pumps only occurred with both a charge and a turn. Notably, more elements are combined as in the upper rows and charges and turns in row 5 were faster than those from all other rows (Fig. S1G).

Analyzing the frequency of row-specific elements in time (Fig. 1G), while ignoring variable nodes 1 and 3 for simplicity (see Methods), revealed a typical sequence of motor events. Before a bout begins, flies stand immobile or charge and turn (Figs. 1G, rows 1, 2, 1Hi-iii). At bout onset, they pump their wings with a charge and turn (Figs. 1G, row 5, 1C, 1Hiv). As a bout progresses, they continue to charge, turn, or stand immobile with their wings elevated (Figs. 1G, rows 3, 4, 1Hv-vii). Finally, after dropping the wings with a charge or turn, they continue to charge, turn, or stand immobile (Figs. 1G, rows 1, 2, 1Hviii, ix). Thus, fly threats contain at least five distinct motor elements that can occur independently or in combination, vary in frequency and speed, and which are expressed in a variable (Fig. S1H), but typical sequence of events. Such multi-motor and oriented threats were often iterated less than 16s apart (Figs. S1I, orange, S1Ji, S1Jii) and interspersed with other behaviors, such as lunges (Chen et al., 2002; Hoyer et al., 2008) or courtship-like unilateral wing extensions (Fig. S1K). Threats also occurred at a distance from targets (~10mm, Fig. S1Lii) suggesting that long-range target cues may evoke this behavior.

Chemosensory cues plus a moving object suffice to evoke threats

To explore the relative roles of male-derived cues and visual motion in threat initiation, we placed solitary, SH WT flies in an arena (Fig. S2A) with a dead male (Fig. 2Ai) and/or a moving dummy (ii, iii), of a size found to be sufficient to elicit social behaviors in other contexts (Agrawal et al., 2014). A dead male or dummy motion alone evoked few threats (Fig. 2Bi, ii). However, both stimuli in combination evoked threats, wing extensions, and lunges (Fig. 2Biii), similar to WT pairs (Fig. S1K). Notably, threats began during dummy motion (Figs. 2E, S2B, D, movie S2). Moreover, unlike wing extensions and lunges (Fig. 2C, middle and bottom), which were mostly directed towards the dead male, threats were only directed toward the moving dummy (Figs. 2C, orange, D, S2C, D). We observed a

decrease in threats at intermediate velocities (Fig. S2C, top); whether this reflects fly extrinsic or intrinsic factors is unclear. Nonetheless, flies paired with a dummy spent as much time threatening targets as WT pairs (Fig. S2E), although dummy evoked threats were comprised of relatively more active motor elements and combinations (Fig. 2F, green) and less immobility (magenta). Interestingly, in the presence of male *Drosophila* cues, we have even observed an active threat towards a heterospecific ant. (Fig. S2F).

To begin to understand the sensory systems involved in these observations, we tested anosmic flies in the presence of a dead male and moving dummy (see Methods) by either surgically removing the antennae from WT flies (Asahina et al., 2014), or by testing genetically anosmic, quad olfactory mutants (*IR8a*, *IR25a*, *OR83b*, *Gr63a*; Ramdya et al., 2014). Consistent with previous results (Wang and Anderson, 2010), we observed that, in these conditions, threats and lunges require a functional olfactory system for their expression (Fig. S2G, columns 1–4). Furthermore, WT flies also threatened a moving dummy in the presence of a CO_2 anesthetized male, arguing against the possibility that threats are promoted by corpse-derived alarm pheromones from dead males (Fig. S2G5; see Methods). With a preliminary understanding of the elemental structure of WT threats and their elicitation by two dissociable sensory cues, chemosensory and visual motion, we turned to finding neurons that mediate this behavior.

Identification of neurons that control threat displays

To understand how the fly nervous system generates threats, we used a Gal4 line (R20E08) that increased threat-like behavior, originally identified in an activation screen for neurons promoting aggression (1/3,000 lines; Hoopfer et al., 2015). Thermogenetic activation of R20E08 neurons using the temperature sensitive ion channel, TrpA1 (Hamada et al., 2008), increased threat expression, as defined by our JAABA classifier, in non-aggressive, group-housed (GH) fly pairs (Figs. 3Bi, S3Aii, Bii). As R20E08 labels many neurons in both the brain and the ventral nerve cord (VNC; Fig. S3Ci), we narrowed down the mediating subset by specifically activating R20E08 neurons labeled in the brain (Figs. S3Aiii, S3Ciii) or in the VNC (Figs. S3Aiv, S3Civ), using Otd-FLP and FLP-ON> or OFF>dTrpA1 effectors (Watanabe et al., 2017). Threats were elevated by thermogenetic activation of R20E08 neurons in the brain, but not in the VNC (Figs. S3Biii vs. iv).

To determine if R20E08 labels neurons required for natural threats, we silenced these neurons in aggressive, single-housed (SH) flies using the inwardly rectifying potassium channel Kir 2.1 (Baines et al., 2001). Silencing all R20E08 neurons (Figs. S3Dii, S3Fii) or only those in the brain (Figs. S3Diii, S3Fiii), significantly reduced threats during natural aggressive interactions (Fig. S3Eii, iii). Together these data suggest that R20E08 brain neurons are sufficient for threat expression when activated, and are necessary for natural threat expression.

To further isolate threat-relevant neurons, we screened many Split-Gal4 hemidrivers (Dionne et al., 2018; Pfeiffer et al., 2010) and found an intersection between the original R20E08 driver (R20E08-DBD) and a second driver (R22D03-AD) that sparsely labeled 2 classes of neurons in the brain (Split^{Thr}, Fig. 3A). Thermogenetic activation of such neurons in pairs of GH flies at 28, 29, and 30° caused a significant temperature-dependent increase in total

threats (Fig. 3Bi, gray column) relative to temperature and genetic controls (Figs. 3Bi, S4A). Notably, no threats were observed at 22°, below the permissive temperature for dTrpA1 ac tivation (Fig. 3Bi). We also observed a temperature dependent decrease in unilateral wing extensions (Fig. 3Bii) but no effect on lunges (Fig. 3Biii).

To determine if threats induced by thermogenetic activation of Split^{Thr} flies are similar to WT threats, we quantitatively compared the two. Like WT threats, we observed charges, turns, and intermittent immobility, before and after a pump as well as extended periods of wing elevation (Figs. 3C, D, movie S3). However, Split^{Thr} activation-induced bouts had fewer pumps, wings were elevated at an average wing angle 8° less than WT (Fig. S4Bi), and bouts lasted longer (Fig. S4Bii). We also observed WT-like 4–6Hz charging in a subset of induced threats (~10%, Fig. S4C) as well as turns toward and away from targets, all in proportions similar to WT flies (Figs. S4D, S1Dii). Also, as in WT flies, pumps, charges, and turns occurred together at the start of a bout (Fig. 3E) and induced threats were comprised of variable numbers of elements; however the median number of pumps per threat was slightly but significantly lower that WT, while the median % time spent elevating the wings during threat was significantly higher (Fig. S4E).

An element space transition diagram (Fig. 3F) revealed that induced threats were comprised of the same elements and element combinations as WT threats. However, we observed relative reductions in some active movements (Fig. 3F, S4F, magenta) and increases in immobility (green). While row 5 pumps were less frequent than in WT, row 5 charges and turns were faster than those in other rows, as in WT flies (Fig. S4Gi, ii). Analyzing the frequency of row-specific elements in time revealed a WT-like sequence of events (Fig. 3G). Thermogenetically induced threats were also iterated (Fig. S4Hi) at a similar distance from targets as for WT flies (Fig. S4Hii). Furthermore, activating these neurons in the presence of a virgin female did not delay copulation (Fig. S4Ii, ii). Thus, despite subtle differences, activating Split^{Thr} neurons in pairs of flies induced threat behavior that is remarkably similar to natural WT threats.

Thermogenetic activation of solitary Split^{Thr} *flies substitutes for male cues and enhances sensitivity to dummy motion*

We next activated Split^{Thr} neurons in solitary GH flies in the presence of a moving dummy. In contrast to WT flies, where a dead male was required for dummy evoked threats (Fig. 2), thermogenetic activation caused dummy-directed threats to occur in the absence of a dead male (Fig. 4Ai, gray columns, 27–30°C). This suggests that artificially induced threats between fly pairs (Fig. 3) are not dependent on counter-threats from the target. Like WT flies (Fig. S2), induced threats occurred during and were oriented towards dummy motion (Figs. 4B, C; S5A, B C; movie S4), and were comprised of both active and immobile elements and combinations (Fig. 4D, S5D). The frequency of row-specific elements in time (Figs. 4E, S5A) revealed that following the onset of dummy motion, flies expressed row 2 elements, followed by row 5 pumps. They then expressed row 3 or row 2 elements, and after the offset of dummy motion, flies exhibited persistent and oriented immobility (Figs. S5Bii, iii, red) with (row 4) or without (row 1) wing elevation.

Interestingly, total threats increased with increasing temperature of thermogenetic activation (Figs. 4Ai, S5A, vertical) as well as with increasing dummy velocity (Fig. S5A, horizontal; DV). At higher temperatures, more threats were evoked by slower moving dummies and vice-versa (Figs. S5B, C), yielding a temperature-dependent increase in the "velocity sensitivity" of thermogenetically induced threats (1/minimum dummy velocity evoking a threat; Fig. 4F). Thus, dummy velocity and the strength of Split^{Thr} thermogenetic activation appeared interchangeable. Unlike WT flies in the presence of a dead male (Fig. 2), Split^{Thr} activation in the absence of a dead male did not induce wing extensions or lunges towards the dummy (Figs. 4Aii, iii), and few threats were observed in the absence of a dummy, even at 30° (Fig. 4G). Thus, thermogenetic activation of Split^{Thr} neurons potentiated dummy-evoked threats, and substituted for the requirement of a dead male to induce dummy-directed threats by WT flies.

Optogenetic activation of Split^{Thr} neurons substitutes for sensory cues and induces different threat motor elements in a threshold-dependent manner

We next activated Split^{Thr} neurons optogenetically using red-shifted opsins, to achieve greater temporal and dynamic range control. Both ReaChR, which has been shown to be a more potent activator than dTrpA1 (Inagaki et al., 2014), and Chrimson (Klapoetke *et al.*, 2014), were equally effective to induce threats with green light but not red light (Fig. S6Ai, ii). Remarkably, GH flies expressing the more sensitive Chrimson in Split^{Thr} neurons exhibited threats in the absence of both a dead male and moving dummy (Fig. 5A-C, movie S5). Induced bouts had fewer pumps, wings were elevated at an average wing angle 9° less than WT flies (Fig. S6Ci), and bouts lasted longer (Fig. S6Cii). As in WT flies however, we observed undirected 4–6Hz charging, but in a much higher percentage of flies (50% vs. 16%, Fig. S6D). We also observed co-occurrence of elements at the start of a bout (Fig. 5D, orange), and variable numbers of elements per threat (Fig. S6E).

A motor element space transition diagram (Fig. 5E) revealed that, as in WT flies, induced threats were comprised of the same elements and element combinations. However, compared to WT, we observed relative reductions in some active elements and increases in active elements with wing elevation and immobility (Fig. 5E, S6F). Although row 5 pumps were less frequent than in WT, such charges were slightly faster than those from other rows (Fig. S6Gi). Furthermore, although threats were optogenetically inducible in the absence of any target object, the frequency of row-specific elements in time (Fig. 5F) revealed a sequence that was strikingly similar to that exhibited by thermogenetically activated flies in response to dummy motion (Fig. 5F, dashed lines).

We next examined how different motor elements of threat depended on photostimulation frequencies (Fig. S6B). At low stimulation frequencies (SF), we often observed charges and turns in the absence of wing pumps or wing elevation (Fig. 5Ci-iii; insets). We quantified the total elements observed during the stimulation period and found that all gradually increased with increasing SF (Fig. S6Hi-iii). An exception was immobility, which did not increase during, but increased following photostimulation (Fig. 5H). Although the SF required to induce particular motor elements varied across individual flies (Fig. 5Gi), different motor elements were evoked in a characteristic order with increasing SF. Indeed, we found that the

median SFs (±SEM, n=40) required to induce particular motor elements were 1Hz for turns (±0.52), 5Hz for charges (±0.78), 10Hz for wing elevation (±1.52) and post-light immobility (±1.88), and 20Hz for wing pumps (±2.36; Figs. 5Gi, S6Ii).

Analysis of all combined photostimulation trials (independent of SF) revealed that activation of Split^{Thr} neurons did not induce motor elements in random and equal combinations. For example, among flies exhibiting combinations of two motor elements, charges plus turns were observed significantly more frequently than were either of those elements in combination with wing elevation (Fig. S6Iii). Consistent with this, threat displays including wing elevation occurred most frequently at SFs higher than those evoking only charges and/or turns (Fig. 5Gii). Thus, optogenetic activation of Split^{Thr} neurons can induce particular motor elements in a threshold-dependent manner.

We next asked if, like thermogenetic activation (Fig. 4), weak optogenetic stimulation could potentiate dummy-evoked threats. Under certain weak stimulation conditions (8 Hz, 1.4 mW/mm^2), we observed a dependence of optogenetically evoked threats on dummy motion (Fig. 5I). Therefore, weaker artificial activation of Split^{Thr} neurons (either thermogenetic or weak opotogenetic) substituted for a dead male but not dummy motion, while stronger (optogenetic) activation substituted for both sensory cues. However, to ensure that the latter optogeneticaly induced threats were not dependent on any visual cues, we activated Chrimson-expressing R20E08 neurons in genetically blind, *norpA*$^-$ flies. In comparison to activation in a *norpA*$^+$ background, we found no difference in the number of induced elements, except for a slight increase in turns (Fig. 5J).

AIP neurons control threat displays

The Split^{Thr} intersection labeled two classes of neurons, those with cell bodies near the Anterior Inferior Protocerebrum (AIP; Yu et al., 2010) and another class located dorsally (Fig. 3A, arrowhead and arrow, respectively). To determine which class mediates optogenetically induced threats, we used a genetic triple intersection combining Split^{Thr}–Gal4 with R21B10-FLP and UAS-FLP-ON>Chrimson, which labeled AIP but not the dorsal neurons (Fig. 6A, arrowhead). 100% of these flies expressed the Chrimson:tdT reporter, in 4–7 AIP neurons per hemi-brain (Fig. 6Bi, ii), with few flies containing any labeled dorsal neurons (Fig. 6Biii), and optogenetic activation induced threats in 100% of GH flies of this genotype (Fig. 6Biv). We also induced a multielement threat with a different triple intersection, Split^{Thr2}–Gal4 (R20E08-AD; R34H05-DBD) combined with R21B10-FLP, which expressed Chrimson in as few as 3 total AIP neurons (Figs. 6Ci, ii; see Methods). Together, these data suggest that AIP Split^{Thr} neurons, and not dorsal neurons, mediate optogenetically induced threats.

We next asked whether cells labeled by our various intersectional drivers are necessary for naturally occurring threats. Silencing with Kir2.1 of neurons labeled by Split^{Thr} strongly reduced threats, without affecting wing extensions or lunges (Fig. 6Di). Similar results were obtained using the reverse version of Split^{Thr}, Split^{Thr3} (R20E08-AD; R22D03-DBD; Fig. 6Dii), which also evoked threats following optogenetic stimulation (Fig. S6J). Since both of these split GAL4 lines label AIP and dorsal neurons (Fig. 6Di, ii, right, arrows), we also tested an AIP-specific triple intersection (Split^{Thr3}; R21B10-FLP; UAS-FLP-ON>Kir; Fig.

6Diii). Silencing with this triple intersection eliminated threats, without significantly reducing lunges or wing extensions (Fig. 6Diii, middle and bottom bar graphs), confirming that AIP neurons are necessary for this behavior. Together, these results indicate that a small cluster of AIP neurons (~3 cells/hemibrain) is sufficient to induce threats when activated, and necessary for natural threats.

Threats function to repel opponents

Male flies use aggression to establish territoriality (Hoffmann, 1987), but the precise contribution of threat displays vs. contact agonistic behavior (e.g., lunging, tussling) to this function has not previously been investigated. Following a threat by a WT conspecific, WT target flies often initiated flight (“take-off”; von Reyn et al., 2014), reflected in an increase in target velocity (V; Fig. 7A, B, movie S6). While some threats co-occurred with large increases in target V (Fig. S7A, red, 18%), others were associated with decreases (orange, 42%) or no large changes (black, 40%). We next divided SH WT pairs (Figs. 1, S1) into winners and losers post-hoc, based on the total threats and lunges exhibited (Fig. 7C, column 1, orange vs. black; rows i, ii; Yurkovic et al., 2006). This revealed that, compared to winners, losers took-off more (Fig. 7Ciii, black bar) and stayed slightly but significantly further away from the center of a food patch (Fig. 7Civ, black bars).

To assess whether artificially induced threats are sufficient to evoke such loser effects, we thermogenetically activated R20E08 neurons in mixed pairs containing a (non-aggressive) GH tester and GH WT target fly. R20E08 activation increased tester threats (Fig. 7C, column 3 vs.1, orange bars), that were associated with changes in target V (Fig. S7B) and which made targets take-off more and stay further from the center of the food (Fig. 7C, column 3, rows iii, iv, black bars). Genetic control testers (Empty (E) Gal4; dTrpA1) paired with WT targets at 30°C exhibited few threats, lunges, or take-offs, and both stayed close to the food (Fig. 7C, column 2). These results indicate that threats in the absence of contact agonistic behaviors are sufficient to repel non-aggressive WT targets, supporting the idea that they function as social signals in the establishment of territoriality (Tinbergen, 1954).

Conversely, to assess if threats are necessary to repel targets, we silenced Split^{Thr3} neurons in SH flies to generate individuals that did not express threats, but which exhibited other aggressive behaviors such as lunging (Fig. 6ii, 7Cii, column 5), and paired them with GH WT flies. While testers with Split^{Thr3} neurons silenced did not express threats, they still made targets take-off and stay away from the food (Fig. 7Ciii, iv, S7C, column 5). Control tester flies expressing mCherry in Split^{Thr3} neurons exhibited threats, lunges, and wing extensions and made targets take-off and stay away from the food (Fig. 7C, column 4, rows iii, iv, S7C). Thus, natural threats are not necessary for SH flies expressing other aggressive behaviors to repel non-aggressive WT targets.

Discussion

We have quantitatively analyzed threats displayed by *Drosophila* and identified a small cluster of neurons that are causal in the expression of this behavior. Several important findings emerge from this analysis. First, fly threats are a combinatorial display of motor elements that are evoked by bimodal sensory cues, and function to repel conspecifics from a

resource or territory. Second, the neural circuits mediating such threats can be cleanly uncoupled from other aggressive behaviors, suggestive of modular organization. Third, varying extents of artificial module activation can substitute for bimodal sensory cues, and induce elements of threat in a scalable, threshold-dependent manner. These data suggest that some complex animal behaviors may be mediated by discrete, scalable brain modules that integrate multi-sensory input to generate variable, functionally relevant motor output.

The elemental structure of threat displays

Fly threats are comprised of at least five distinct motor elements that each involve particular movements or postures of the legs and wings. Charges and turns are independent elements that can occur with a periodicity (4–6Hz) that is independent of target motion and are likely mediated by an unknown pattern generator (Kristan et al., 2005). Threatening flies can iterate directed turns in as little as 150ms, a mode of social orientation that resembles saccadic flight maneuvers (Collett and Land, 1975) and one that appears distinct from the smooth pursuit observed in other contexts (Agrawal et al., 2014; Clowney et al., 2015). Flies initiate threats by executing wing pumps in combination with charges and turns that rapidly (~60ms) inflate the apparent size of threateners to roughly 400% in azimuth (Dierick, 2007). Such pumps are typically followed by bilateral wing elevation that can be combined with charges, turns, and bouts of immobility. Lastly, flies exhibit oriented and intermittent immobility before, during, and after threats, a phenomenon that resembles “active freezing” (Gibson et al., 2015).

Although threat motor elements can vary in the frequency and speed at which they are expressed, they nevertheless have a constancy of form and follow a typical sequence (Morris, 1957). Indeed, most threat bouts begin with a rapid pump, a looming visual cue that can evoke take-offs in target flies (von Reyn et al., 2014). Visual object motion evokes active threat elements (Fig. 2F), suggesting that variance in threat motor output could be explained by variance in target-derived motion cues, as shown directly for courtship song in flies (Coen et al., 2016). However, such variance may also reflect intrinsic variation in the level of activity within circuits mediating graded sensory-motor transformations (Heiligenberg, 1974). In any case, variable threats that evoke variable target responses, could lead to further variation in threat expression (Lange and Leimar, 2003; Stokes, 1962).

A brain module for threat displays

Threat displays are closely linked to and often precede other contact aggressive behaviors such lunging, tussling, and boxing (Alekseyenko et al., 2014; Asahina et al., 2014; Chen et al., 2002; Hoffmann, 1987). Although threats are easily distinguishable by human observers from other aggressive actions, this does not necessarily imply that the neural control of threats must be organized separately from that of other agonistic behaviors. Here we show that the neural circuits underlying threats can be cleanly uncoupled from other types of agonistic behavior in *Drosophila*. Indeed, we isolated as few as 3 total AIP neurons that, when activated, specifically promote naturalistic threat displays. Importantly, silencing this cluster eliminated threat displays without interfering with other types of agonistic behavior, such as lunging (Figs. 6D and 7C). Although WT and induced threats are remarkably similar, they differ subtly in the frequency and amplitude of elements expressed. These

differences could reflect an inability to precisely replicate natural patterns of AIP activity, or that Split^{Thr} lacks relevant or labels irrelevant cells. In any case, our data demonstrate that threats are neurally dissociable from other aggressive behaviors, implying that AIP neurons constitute a genetically and anatomically distinct brain module for threat displays and that threats are encoded separately from, rather than as part of a continuum with, other aggressive behaviors.

Modular neural systems that generate complex behaviors appear to be common (de Boer et al., 2015; Xu et al., 2012; Yang and Shah, 2014). Indeed, it has long been suggested that repertoires of behavior are mediated by modular, hierarchically organized “nerve centres” (Baerends, 1976; Dawkins, 1996; Tinbergen, 1950). More specifically, Tinbergen hypothesized that aggression, mating, and nesting are all controlled by a hierarchically superordinate “reproductive” module (Fig. S7D, Level 1). According to this model, activation of an aggression module (Fig. S7D, Level 2) would activate a threat and/or contact aggression (“Lunge”) module (Fig. S7D, Level 3). Activation of a threat module would, in turn, generate threat-specific motor elements (Fig. S7D, Level 4). As AIP neurons do not promote lunging (Figs. 3Biii, 4Aiii, 6) or other contact agonistic behaviors, they appear to constitute a “Level 3” threat module in a Tinbergian scheme.

Are aggression circuits hierarchically organized? Such a hierarchy would predict that AIP neurons are post-synaptic and functionally downstream of neurons that promote aggression more broadly. Activation of aSP6 central brain neurons promotes the full aggressive repertoire, including threats, lunges, and tussling (Asahina et al., 2014), suggesting that these neurons may constitute a “superordinate” aggression module (Fig. S7D, Level 2). While aSP6 and AIP fibers are in close proximity, as revealed by GRASP (Fig. S7F; Aso et al., 2014; Gordon and Scott, 2009), our efforts to link the two populations functionally have thus far been unsuccessful. Interestingly, while aSP6 neurons are FruM^{+} and male-specific, AIP neurons are not (Fig. S7E), and may mediate female as well as male threat displays (Chan and Kravitz, 2007). Thus, while the function and anatomy of aSP6 and AIP neurons are suggestive, it remains an open question as to whether aggression in *Drosophila* is indeed mediated hierarchically.

The ethological function of threat displays

Aggression involves many distinct actions, making it difficult to ascertain their corresponding evolutionary or behavioral functions (Tinbergen, 1963). Nevertheless it has been suggested that threat displays serve a social communication function (Tinbergen, 1954). Here we have exploited our ability to selectively add or delete threats from dyadic social encounters between *Drosophila* males to ascertain the function of this behavior. Our selective addition of threats to otherwise non-aggressive males directly demonstrates that threats can facilitate territorial repulsion in the absence of other agonistic behaviors. However, this repulsion was not as strong as that elicited by WT males exhibiting the full aggressive repertoire. Conversely, selective deletion of threats from aggressive males only mildly reduced the efficacy of target repulsion.

Together, these data suggest that different aggressive behaviors may cooperate redundantly to repel conspecifics (Andersson, 1980; Blurton Jones, 1968) and to establish dominance,

perhaps through the induction of a “loser” status in subordinate flies (Yurkovic et al., 2006). They also provide evidence that threats could be utilized, in principle, to repel conspecific competitors in the absence of other aggressive behaviors, as during a stand-alone or “bluff” threat (Maynard Smith, 1979). However, as the cues that generate threats in *Drosophila*, also generate other aggressive behaviors (Fig. 2B), fly threats may be “honest” signals of a readiness to attack if necessary (Hurd and Enquist, 2001).

Multi-sensory integration and the expression of threat displays

We found that threat expression in WT flies could be evoked by two dissociable classes of sensory cues: small object visual motion (Wu et al., 2016), and cues derived from male flies, which are likely chemosensory (de la Paz Fernández et al., 2010; Fernández and Kravitz, 2013; Wang and Anderson, 2010; Wang et al., 2011). Indeed, flies lacking a functional olfactory system did not perform threats toward a moving object, indicating that olfactory signals are required; however, gustatory cues may also be involved. One possibility is that each cue contributes to threat expression differently. For example, male-derived chemosensory cues may induce a covert “tendency”, or increased probability to perform a behavior (Heiligenberg, 1974; Hinde, 1955), that is triggered, or “released” by visual motion (Fig. 7D, blue, green; Aguilar-Argüello et al., 2015; Tinbergen, 1954).

How do these sensory cues relate to the function of AIP neurons? Interestingly, weak optogenetic or thermogenetic AIP activation could substitute for chemosensory but not visual motion cues, while strong optogenetic activation substituted for both. Moreover, gradual increases in thermogenetic AIP activation caused a graded lowering of the threshold for motion-released threats (Fig. 4F), implying that AIP activation and visual motion are functionally equivalent. Together, these data suggest that AIP neurons may integrate male cues and visual motion, and that these two modalities could be weak vs. strong drivers of AIP neuronal activity, respectively (Fig. 7D, 7Ei). Unfortunately, experiments to detect activation of AIP neurons by either male or motion cues using 2-photon calcium imaging in head-fixed flies have thus far yielded negative results. We thus cannot exclude that the integration of one or both stimulus modalities occurs upstream or downstream of AIP neurons (Fig. 7Eii, iii). Nevertheless, AIP dendrites (Fig. S7G, magenta) project into the lateral protocerebral complex, a brain region that receives multi-sensory inputs and which is involved in many social behaviors (Asahina et al., 2014; Watanabe et al., 2017; Yu et al., 2010).

Analogously, female and visual cues are known to promote object following by male flies (Agrawal et al., 2014; Kohatsu et al., 2011), and P1 neurons, which are involved in male courtship behavior (von Philipsborn et al., 2011; Yamamoto and Koganezawa, 2013), are activated by pheromonal cues and gate visual input to themselves (Kohatsu and Yamamoto, 2015). Perhaps AIP neurons play an analogous role in the multi-sensory control of threat.

AIP neurons control threat motor elements in a scalable manner

Our results suggest that AIP cells control threat displays in a scalable, or graded, manner, according to their level of activity. It has long been observed that many complex behaviors appear as less intense versions of their complete expressions, known classically as “intention

movements" (Daanje, 1951; Heinroth, 1911). Similarly, the escalating combinatorial complexity and intensity of motor elements expressed during WT threats (Fig. 1F, rows 1–5) can be recapitulated by varying the threshhold intensities of artificial activation (Fig. 5G). Charges and turns often appear before complete WT displays (Fig. 1F, row 2) and can be induced alone by mild optogenetic AIP activation, suggesting that they are relatively low threshold elements (Fig. 7D, yellow, orange). Likewise, wing elevation, pumps, and persistent immobility (Fig. 1F, rows 3, 5, 1, 4) can be optogenetically induced at high stimulation frequencies, implying they are relatively high threshold motor elements (Fig. 7D, pink, dark red, dark blue).

These observations suggest that the expression of different threat motor elements depends on the level of activity in the AIP module (Fig. 7D; Dawkins, 1996; Kennedy et al., 2014). If so, then AIP cells appear to combine classic ideas of modular organization (Tinbergen, 1950) with the concept of scalable motor output controlled by a graded "hydraulic" drive (Lorenz, 1981). Such a circuit could provide a mechanism to transform graded multi-sensory input into a set of specific motor elements that can be coordinated into a characteristic action pattern, while affording flexibility in their combinatorial implementation.

In some respects, the properties of AIP neurons may seem similar to those of P1 neurons, which mediate higher order control of wing extension and song production in *Drosophila* males (von Philipsborn et al., 2011; Yamamoto et al., 2014). However, unlike AIP neurons, which elicit a single type of social behavior (threat), P1 cells can induce multiple courtship-related behaviors like wing extensions, tapping, and licking (Kohatsu et al., 2011), and can also indirectly trigger aggression, an opponent social behavior (Hoopfer et al., 2015; Koganezawa et al., 2016). Downstream of P1, pIP10 and P2b descending interneurons specifically mediate wing extension and song production (von Philipsborn et al., 2011; Yamamoto et al., 2014), perhaps more analogous to AIP cells. However, in contrast to AIP, pIP10 activation appears to trigger song in an all or nothing manner (von Philipsborn et al., 2011) and biases mutually exclusive song modes independent of the strength of stimulation (Clemens et al., 2017).

Potential generality of scalable modules

Threats have been elicited in chickens, cats, and monkeys following artificial brain stimulation (Hess and Briggier, 1943; Lipp and Hunsperger, 1978; von Holst and von Saint Paul, 1962). Whether these effects reflect the activation of scalable modules such as described here is not clear. Studies in the murine ventromedial hypothalamus (VMH) have provided evidence of genetically distinct cell populations whose optogenetic activation controls social (Lee et al., 2014) or defensive (Kunwar et al., 2015, Wang et al. 2015) behaviors in a scalable manner, suggesting that scalable modules may be a general feature of neuro-behavioral control across phylogeny (Kennedy et al. 2015). However, in those cases, different levels of stimulation evoked different behaviors (e.g., freezing vs. flight, mounting vs. attack), rather than low- vs. high-intensity elements of the same behavior. Furthermore, no evidence was presented to relate the effect of artificial stimulation to the intensity or modality of specific sensory inputs, as shown here. Our data provide evidence of a neural module that may transform variable multi-sensory input into scalable, threshold-dependent

variable motor output. Future studies should investigate the circuit mechanisms underlying such multisensory integration and the threshold-dependence of the motor elements comprising threat, a behavior with self-evident relevance to human social interactions.

STAR METHODS

CONTACT FOR REAGENT AND RESOURCE SHARING

Requests for further information or resources should be directed to David J. Anderson (wuwei@caltech.edu)

EXPERIMENTAL MODEL AND SUBJECT DETAILS

Behavior arenas and fly rearing—Experiments were performed in the arenas described (Figs. S1A, S2A). Modified Heisenberg chambers (Hoyer et al. 2008) were constructed (Caltech machine shop) with floors made of white plastic and walls and a lid made of transparent plastic. Walls were coated with insect-a-slip (BioQuip Products) to keep flies from climbing on them. In all cases, arenas contained a centralized food patch made from 2.5% (w/v) sucrose and 2.25% (w/v) agarose in apple juice. For Fig. S2A, chambers were suspended off the side of a desk. A custom stand (B.J.D) for a stepper motor (SX09238, Cana Kit) was placed underneath. The motor was controlled with Matlab (Mathworks) via an Arduino UNO microcontroller (Arduino). A propeller (Caltech machine shop) mounted to the rotor, rotated a large actuating magnet (D8X0BR, K&J magnetics) that, in turn, moved (actuated) a small, black painted, fly sized magnet (D101-N52, K&J magnetics) inside the arena. Arenas were illuminated with white LEDs.

Wild-type Canton-S male flies, maintained on a 9AM:9PM light:dark cycle, were collected on CO_2 shortly after eclosion and reared in isolation (one fly per vial, single-housed (SH), “aggressive”; Figs. 1, 2, S3D-F, 6D, 7C), or in a group (~20 individuals per vial, group-housed (GH), “non-aggressive”; Figs. 3, S3A-C, 4, 5, 7C) at 25°C, or as otherwise indicated. Seven day old individuals were gently aspirated into the chamber and all experiments, except where indicated, were performed at 25°C. Videos (Fig. 1) lasted 15 minutes per pair. For experiments in Fig. 2, freeze killed males were fixed on the food, and live tester flies were allowed to acclimate in the chamber for 2 minutes before starting video acquisition. For olfactory ablations, we removed the 3rd antennal segment (Fig. S2Gii) from flies under CO_2 anesthesia with forceps 3 days post eclosion (Asahina et al., 2014). Mock removal (Fig. S2Gi) consisted of prodding this segment on anesthetized flies with a paintbrush. We also used a quad olfactory mutant (Fig. S2Giii; *IR8a*, *IR25a*, *OR83b*, *Gr63a,* (Ramdya et al., 2014; Ana Silbering and Richard Benton) and as a genetic control, crossed these flies to WT to generate heterozygous mutants (Fig. S2Giv). For Fig. S2Gv we partially embedded a male fly under CO_2 anesthesia into the food agarose and held it down with a paintbrush until the agarose cured.

METHODS DETAILS

Thermogenetic activation—Experiments were performed in the arenas described (Figs. S1A, S2A). Male flies for dTrpA1 activation were collected on CO_2 shortly after eclosion and reared as a group (~20 individuals, GH) at 22°C for 7 days. Fli es were then

preincubated for 15 minutes in the temperature controlled room where the experiments took place. Temperature, as indicated (Figs. 3, S3, 4, S4, S5), was verified and measured with an IR thermometer (Nubee) pointed at the floor of the arena (lid off). Videos (Figs. 3, S3B) lasted 10 minutes per pair.

Optogenetic activation—Experiments were performed in the arena described (Fig. S6A). The camera was equipped with an IR longpass filter (LP780–25.5, Midwest Optical Systems, Inc.) and a transparent plastic floor was coated underneath with a thin layer of white acrylic paint and backlit with 850nm IR LEDs. We used 685nm red stimulation LEDs (FD-14R-Y1, www.ledfedy.com), powered with a DC power supply (Mastech), wired to a 1000mA buck puck driver (3021-D-E-1000, Luxeon Star). LEDs were computer controlled via an analog device (USB 1208FS-plus, Measurement Computing) and intensity measurements were made with a light-meter (S130VC, Thorlabs) as indicated in Fig. S6A. Grown in the dark, male flies for Chrimson activation were collected on CO_2 shortly after eclosion and reared as a group (~20 individuals, GH), in the dark at 25°C. Flies were then transferred to a vial containing half a compacted Kim wipe and 1ml of a solution containing 100mM sucrose and 0.8mM all *trans*-Retinal (Sigma-Aldrich) for 48 hours prior to testing. Seven day old flies were tested at 25°C. For Fig. S6Aii, we photostimulated flies of the indicated genotypes in 12 well chambers (Asahina et al., 2014) with 2 different wavelengths (LEDs from Luxeon Star placed directly above the chambers). The experimental intensities in mW/mm^2 were 0.12 for 530nm and 0.39 for 685nm. For Fig. 5I, we tested flies with 40Hz light, then moved the dummy, then stimulated with 8Hz light, then stimulated with 8Hz light while moving the dummy, and then repeated the latter two stimulus conditions again. Data were pooled for 8Hz light and light plus dummy conditions. Flies for triple intersections (Figs. 6A-C) were 10 days old when tested.

Neuronal silencing—Experiments were performed in the arena described (Fig. S1A). Male flies for Kir silencing were collected on CO_2 shortly after eclosion and reared in isolation (SH) at 25°C for 7 days. Flies were then tested at 25°C and videos (Figs. S3D-F, 6D) lasted 15 minutes per pair. We utilized $Split^{Thr3}$ as opposed to $Split^{Thr}$, for the triple intersection as it had stronger Kir expression (Fig. 6D).

Mixed pair experiments—For mixed pair experiments in Fig. 7, tester flies in columns 2 and 3 were marked with a small but identifiable slice removed with a razor blade from the tip of one wing. For columns 4 and 5, tester or target flies were marked with a minimal, white dot of paint on the dorsal thorax. In all cases, only one fly was marked and identities were maintained throughout. Videos (Fig. 7) lasted 15 minutes per pair.

Immunohistochemistry—Intact fly brains or ventral nerve cords were dissected in PBS and fixed in 4% formaldehyde in PBS for 2 hours at 4°C. After washe s with 0.05% TritonX-100 in PBS (30 minutes x3), samples were blocked with 10% normal goat serum in PBS for 2 hours. Samples were incubated in primary antibody diluted in blocking solution for 1–3 days. Samples were washed with 0.05% TritonX-100 in PBS (30 minutes x3) and blocked in 10% normal goat serum in PBS for 2 hours. Samples were then incubated in secondary antibody, diluted in blocking solution, for 1–3 days. Following washes with

0.05% TritonX-100 in PBS (30 minutes x3) samples were incubated overnight in Vectashield (Vector Laboratories) and mounted on glass slides. Images were taken with an Olympus FV-1000 confocal microscope and processed with Fiji (https://fiji.sc/). Despeckling and sharpening were applied to maximum intensity Z-stacks.

We utilized the following anti-bodies: rabbit anti-DsRed (1:1000, #632496, Clontech), mouse nc82 (1:10, Developmental Studies Hybridoma Bank, University of Iowa), mouse anti-GFP (1:1000, A11120, Thermo Fisher Scientific), rabbit anti-GFP (1:1000, A11122, Thermo Fisher Scientific), Goat anti-mouse Alexa Flour 488 (1:1000, A-11001, Thermo Fisher Scientific), Goat anti-rabbit Alexa Flour 488 (1:1000, A-11008, Thermo Fisher Scientific), Goat anti rabbit Alexa Flour 568 (1:1000, A-11011, Thermo Fisher Scientific), Goat anti mouse Alexa Flour 633 (1:1000, A-21050, Thermo Fisher Scientific), Rabbit anti FruM (1:3000, Barry Dickson), Rat anti N-cadherin (1:30, Developmental Studies Hybridoma Bank, University of Iowa).

QUANTIFICATION AND STATISTICAL ANALYSIS

Fly tracking and behavior classification—Pairs of flies were recorded at 60 frames per second with a camera (Flea3, FL3-U3–13Y3M-C, Point Grey) and Bias acquisition software (Will Dickson, IO Rodeo). Flies were tracked with the Caltech Fly Tracker software (Eyrun Eyjolfsdottir and Pietro Perona). Behaviors were classified using JAABA (Kabra et al. 2012), where classifiers were trained manually for each behavior on a ground-truth data set of 12 videos. Predicted positives were screened manually using software written in Matlab (Talmo Pereira). The resulting accuracy metrics, precision and recall (Eyrun Eyjolfsdottir and Pietro Perona; Hoopfer et al. 2015), were calculated for each behavior using 11 additional videos. For each behavior, such bout-wise metrics were as follows: Threat display (precision, 92%; recall, 96%), wing extension (precision, 91%; recall, 94%), lunge (precision, 89%; recall, 93%), take-off (precision, 75%; recall, 86%). Classifiers were trained with additional data in cases where solitary flies were with a dummy to eliminate false positives generated by the dummy. Also, classifiers were re-trained for optogenetic experiments to eliminate the dependence of the classifier on inter-fly features. All classifiers were applied equally across experimental and control genotypes.

Statistics and Quantification—All analyses were performed using custom software written in Matlab. Statistical analyses were performed using non-parametric pairwise Mann-Whitney U tests, multiple comparison tests, and 1-way ANOVAs as indicated. Classified threats were aligned according to the maximum wing angular velocity (Fig. 1C, t=0). A “bout” was defined as periods when the wings were extended or elevated and a “threat” was defined as a bout +/− 0.5s. A threat display may last longer (Fig. S1C) but we adopted this convention here to include some, but not all, pre bout charging and immobility while also limiting contamination from prior bouts (Fig. S1I). Thresholds (Fig. 1D) were designated as those which captured relevant features after visual inspection of all threats. Typically, transition diagrams have been utilized to describe transitions between discreet events. However, the kinematics of threat displays are multi-motor and continuous, leading us to apply thresholds to parse such displays into discreet and binary events. Pumps are easily identifiable and are identified by average wing angles above 65 degrees. No other events in

the time window surrounding classified threats have this property. Wing elevation angle may vary slightly during a single threat and between threats (see Fig. S1Bi). The thresholds for wing elevation were thus selected to encapsulate the majority of such events. Charges and turns are discreet events and thresholds were selected to exclude bouts of continuous walking or smooth turning. This is similar to thresholding performed for analyzing fly saccades in flight (Bender and Dickinson, 2006). Thresholds for immobility were selected to identify periods in our videos which, despite some noise in the tracking, appear as freeze frames to a human observer.

Thresholded data was assigned a number in “element space” (Fig. 1Ei) and an ordered vector of such values for each threat was used to compute the transition probabilities in element space (Fig. S1F). Flies spent from one frame (16.67ms) to many frames in a particular node. We constructed a transition diagram (Fig. 1F), excluding self-transitions, with nodes that are proportional to element frequency in element space (Fig. 1Eii). Exclusions established in 1Eiii were maintained throughout. Nodes 1 and 3 contained variable bouts of slower walking and turning, some irregular movements, and node 1 also contained cases where only 1 wing was raised (see also Fig. 4C; Jacobs, 1960). We largely ignored discussing these nodes in favor of highlighting the most obvious motor elements.

Transition diagrams (Figs. 1F, 2F, 3F, 4D, 5E) were constructed from classified threats using the same thresholds in exactly the same manner, were scaled relative to Fig. 1F, and further scaled as indicated to fit the figure. Differences between diagrams were calculated by subtracting WT threat values from data where indicated (Figs. 2G, S4F, S5D, S6F). Data points were then assigned to rows according to the transition diagrams. The frequency of each row in time was plotted for classified threats (Figs. 1G, 3G) or plotted using all data, independent of classification, during object motion (Fig. 4E) or photostimulation (Fig. 5F). We conducted Fourier analyses to quantify periodicity in velocity data and selected a subset, with a maximum >1Hz power in the 4–7Hz range and above the mean (Fig. S1C, S4C, S6D). Elements were also quantified (Figs. S1E, G, S4E, G, 5G, H, S6E, G, H, I) according to the thresholds indicated (Fig. 1D). WT and induced threats were treated with exactly the same analyses where applicable. We pooled (Figs. 5G, H, S6H, I) and quantified data from the two highest stimulation intensities (Fig. S6B). For Figs. 5G and S6I, thresholds from Fig. 1 were applied to all trials and those positive for turns and charges contained at least 4 of such spikes whereas trials positive for wing elevation had such a pose for > 10% of the trial. Fig. S2F is an observation following the introduction of an ant into an arena with 4 flies that had exhibited some prior aggression. Fig. 6C was one individual (N=15), from a stochastic triple intersection, that labeled 3 total AIP neurons and displayed a light induced threat.

DATA AND SOFTWARE AVAILABILITY

The software used in this study includes Bias acquisition software (Will Dickson, IO Rodeo, https://bitbucket.org/iorodeo/bias/src/default/), FlyTracker (Eyrun Eyjolfsdottir and Pietro Perona, http://www.vision.caltech.edu/Tools/FlyTracker/), and JAABA (Kabra et al., 2013).

Supplementary Material

Refer to Web version on PubMed Central for supplementary material.

Acknowledgements

We thank Gerry Rubin for sharing unpublished reagents (see Key Resources Table); Talmo Pereira for classification code; Kiichi Watanabe for performing the experiments in Fig. S7E; Hidehiko Inagaki for sharing R21B10-FLP; Jon Schor, Ruohan Wang, Alberto Corona, Michael Altermatt, Jared Everson (students); Yonil Jung, Peter Weir, Michael Dickinson, Mhemet Keles, and Mark Frye for help with Ca^{2+} imaging experiments; Kavya Sreedhar, Luciana Hartmann, Romann Webber, Yisong Yue for assistance with transition diagrams; Evan Tanner for SV1 code; Ana Silbering and Richard Benton for quad olfactory mutants; Barry Dickson for FruM anti-body; and Anderson lab members who provided expertise and comments. B.J.D was a Life Sciences Research Foundation fellow for the Ellison Medical Foundation. D.J.A is an Investigator of the Howard Hughes Medical Institute.

References

Agrawal S, Safarik S, and Dickinson M (2014). The relative roles of vision and chemosensation in mate recognition of *Drosophila melanogaster*. J. Exp. Biol 217, 2796–2805. [PubMed: 24902744]

Aguilar-Argüello S, Díaz-Fleischer F, and Rao D (2015). Target-invariant aggressive display in a tephritid fly. Beh. Proc 121, 33–36.

Alekseyenko OV, Chan Y-B, de la Paz Fernandez M, Bülow T, Pankratz MJ, and Kravitz EA (2014). Single serotonergic neurons that modulate aggression in *Drosophila*. Curr. Biol 24, 2700–2707. [PubMed: 25447998]

Anderson DJ, and Perona P (2014). Toward a Science of Computational Ethology. Neuron 84, 18–31. [PubMed: 25277452]

Andersson M (1980). Why are there so many threat displays? J. Theor. Biol 86, 773–781. [PubMed: 7195963]

Asahina K, Watanabe K, Duistermars BJ, Hoopfer ED, González CR, Eyjólfsdóttir EA, and Perona PADJ (2014). Tachykinin-expressing neurons control male-specific aggressive arousal in *Drosophila*. Cell 156, 221–235. [PubMed: 24439378]

Aso Y, Sitaraman D, Ichinose T, Kaun KR, Vogt K, Belliart-Guérin G, Plaçais P-Y, Robie AA, Yamagata N, Schnaitmann C, et al. (2014). Mushroom body output neurons encode valence and guide memory-based action selection in *Drosophila*. eLife 3, e04580. [PubMed: 25535794]

Baerends GP (1976). Functional Organization of Behavior. Animal Behaviour 24, 726–738.

Baines RA, Uhler JP, Thompson A, Sweeney ST, and Bate M (2001). Altered Electrical Properties in *Drosophila* Neurons Developing without Synaptic Transmission. J. Neuro 21, 1523.

Bender JA, and Dickinson MH (2006). Visual stimulation of saccades in magnetically tethered *Drosophila*. J. Exp. Biol 209, 3170–3182. [PubMed: 16888065]

Blurton Jones NG (1968). Observations and Experiments on Causation of Threat Displays of the Great Tit (*Parus major*). Animal Behaviour Mon. 1, 73–158.

Chan YB, and Kravitz EA (2007). Specific subgroups of FruM neurons control sexually dimorphic patterns of aggression in *Drosophila melanogaster*. PNAS 104, 19577–19582. [PubMed: 18042702]

Chen P, and Hong W (2018). Neural Circuit Mechanisms of Social Behavior. Neuron 98, 16–30. [PubMed: 29621486]

Chen S, Lee AY, Bowens NM, Huber R, and Kravitz EA (2002). Fighting fruit flies: a model system for the study of aggression. PNAS 99, 5664–5668. [PubMed: 11960020]

Clemens J, Coen P, Roemschied F, Pereira T, Mazumder D, Pacheco D, and Murthy M (2017). Discovery of a new song mode in *Drosophila* reveals hidden structure in the sensory and neural drivers of behavior. bioRxiv.

Clowney EJ, Iguchi S, Bussell JJ, Scheer E, and Ruta V (2015). Multimodal Chemosensory Circuits Controlling Male Courtship in *Drosophila*. Neuron 87, 1036–1049. [PubMed: 26279475]

Coen P, Xie M, Clemens J, and Murthy M (2016). Sensorimotor transformations underlying variability in song intensity during *Drosophila* courtship. Neuron 89, 629–644. [PubMed: 26844835]

Collett TS, and Land MF (1975). Visual control of flight behaviour in the hoverfly, *Syrittapipiens L*. J. Comp. Physiol 99, 1–66.

Craig W (1917). Appetites and Aversions as Constituents of Instincts. PNAS 3, 685–688. [PubMed: 16586767]

Daanje A (1951). On Locomotory Movements in Birds and the Intention Movements Derived From Them. Behaviour 3, 48–98.

Darwin C (1873). The expression of the emotions in man and animals (Murray).

Dawkins R (1996). Hierarchical Organization: A candidate principle for ethology In Growing points in Ethology (Cambridge University Press). Bateson PPG & Hinde RA (Eds.).

de Boer SF, Olivier B, Veening J, and Koolhaas JM (2015). The neurobiology of offensive aggression: Revealing a modular view. Physiology and Behavior 146, 111–127. [PubMed: 26066717]

de la Paz Fernández M, Chan YB, Yew JY, Billeter JC, Dreisewerd K, Levine JD, and Kravitz EA (2010). Pheromonal and behavioral cues trigger male-to-female aggression in *Drosophila*. PLoS Biol. 8, e1000541. [PubMed: 21124886]

Dierick HA (2007). A method for quantifying aggression in male *Drosophila melanogaster*. Nat. Prot 2, 2712–2718.

Dionne H, Hibbard KL, Cavallaro A, Kao JC, and Rubin GM (2018). Genetic Reagents for Making Split-GAL4 Lines in *Drosophila*. Genetics 209, 31–35. [PubMed: 29535151]

Dow MA, and von Schilcher F (1975). Aggression and mating success in *Drosophila melanogaster*. Nature 254, 511–512. [PubMed: 804664]

Emlen JT (1962). The Display of the Gorilla. PAPS 106, 516–519.

Emmons SW (2018). Neural Circuits of Sexual Behavior in *Caenorhabditis elegans*. Annu. Rev. Neurosci 41, 349–369 [PubMed: 29709211]

Fernández MP, and Kravitz EA (2013). Aggression and courtship in *Drosophila*: pheromonal communication and sex recognition. J. Comp. Phys. A 199, 1065–1076.

Gibson WT, Gonzalez CR, Fernandez C, Ramasamy L, Tabachnik T, Du RR, Felsen PD, Maire MR, Perona P, and Anderson DJ (2015). Behavioral Responses to a Repetitive Visual Threat Stimulus Express a Persistent State of Defensive Arousal in *Drosophila*. Curr. Biol 25, 1401–1415. [PubMed: 25981791]

Gordon MD, and Scott K (2009). Motor control in a *Drosophila* taste circuit. Neuron 61, 373–384. [PubMed: 19217375]

Hamada FN, Rosenzweig M, Kang K, Pulver SR, Ghezzi A, Jegla TJ, and Garrity PA (2008). An internal thermal sensor controlling temperature preference in *Drosophila*. Nature 454, 217–220. [PubMed: 18548007]

Hashikawa K, Hashikawa Y, Falkner A, and Lin D (2016). The neural circuits of mating and fighting in male mice. Curr. Op. Neurobiol 38, 27–37. [PubMed: 26849838]

Heiligenberg W (1974). Processes Governing Behavioral States of Readiness In Advances in the Study of Behavior (Academic Press) Lehrman DS, Rosenblatt JS, Hinde RA, and Shaw E, (Eds.) 173–200.

Heinroth O (1911). Beiträge zur Biologie, namentlich Ethologie und Psychologie der Anatiden (Verhandlungen des 5 Internationalen Ornithologen-Kongresses Berlin).

Hess WR, and Briggier M (1943). Das subkortikale Zentrum der affektiven Abwehrreaktion. Helv. Physiol. Acta 1, 33–52.

Hinde RA (1955). A comparative study of the courtship of certain finches (*Fringillidae*). Ibis 97, 706–745.

Hoffmann AA (1987). A laboratory study of male territoriality in the sibling species *Drosophila melanogaster* and *D. simulans*. Animal Behaviour 35, 807–818.

Hoopfer ED, Jung Y, Inagaki HK, Rubin GM, and Anderson DJ (2015). P1 interneurons promote a persistent internal state that enhances inter-male aggression in *Drosophila*. eLife 4, e11346. [PubMed: 26714106]

Hoyer SC, Eckart A, Herrel A, Zars T, Fischer SA, Hardie SL, and Heisenberg M (2008). Octopamine in male aggression of *Drosophila*. Curr. Biol 18, 159–167. [PubMed: 18249112]

Hurd PL, and Enquist M (2001). Threat display in birds. Can. J. Zool 79, 931–942.

Inagaki HK, Jung Y, Hoopfer ED, Wong AM, Mishra N, Lin JY, Tsien RY, and Anderson DJ (2014). Optogenetic control of freely behaving adult *Drosophila* using a red-shifted channelrhodopsin. Nat. Meth 11, 325–332.

Jacobs ME (1960). Influence of light on mating of *Drosophila melanogaster*. Ecol. 41, 182–188.

Kabra M, Robie AA, Rivera-Alba M, Branson S, and Branson K (2012). JAABA: interactive machine learning for automatic annotation of animal behavior. Nat. Meth 10, 64–67.

Kennedy A, Asahina K, Hoopfer ED, Inagaki HK, Jung Y, Remedios R, and Anderson DJ (2014). Internal States and Behavioral Decision-Making: Toward an Integration of Emotion and Cognition. CSH Symp. Quant. Biol 79, 199–210.

Klapoetke NC, Murata Y, Kim SS, Pulver SR, Birdsey-Benson A, Cho YK, Morimoto TK, Chuong AS, Carpenter EJ, Tian Z, et al. (2014). Independent Optical Excitation of Distinct Neural Populations. Nat. meth 11, 338–346.

Koganezawa M, Kimura K. i., and Yamamoto D (2016). The neural circuitry that functions as a switch for courtship versus aggression in *Drosophila* males. Curr. Biol 26, 1395–1403. [PubMed: 27185554]

Kohatsu S, Koganezawa M, and Yamamoto D (2011). Female Contact Activates Male-Specific Interneurons that Trigger Stereotypic Courtship Behavior in *Drosophila*. Neuron 69, 498–508. [PubMed: 21315260]

Kohatsu S, and Yamamoto D (2015). Visually induced initiation of *Drosophila* innate courtship-like following pursuit is mediated by central excitatory state. Nat. Comm 6, 6457

Krakauer JW, Ghazanfar AA, Gomez-Marin A, MacIver MA, and Poeppel D (2017). Neuroscience Needs Behavior: Correcting a Reductionist Bias. Neuron 93, 480–490. [PubMed: 28182904]

Kristan WB, Calabrese RL, and Friesen WO (2005). Neuronal control of leech behavior. Prog. Neurobiol 76, 279–327. [PubMed: 16260077]

Kunwar PS, Zelikowsky M, Remedios R, Cai H, Yilmaz M, Meister M, and Anderson DJ (2015). Ventromedial hypothalamic neurons control a defensive emotion state. eLife 4, e06633.

Lange H, and Leimar O (2003). The function of threat display in wintering great tits. Animal Behavior 65, 573–584.

Lee H, Kim DW, Remedios R, Anthony TE, Chang A, Madisen L, Zeng H, and Anderson DJ (2014). Scalable Control of Mounting and Attack by ESR1(+) Neurons in the Ventromedial Hypothalamus. Nature 509, 627–632. [PubMed: 24739975]

Lipp HP, and Hunsperger RW (1978). Threat, Attack and Flight Elicited by Electrical Stimulation of the Ventromedial Hypothalamus of the Marmoset Monkey *Callithrix jacchus*. Brain, Behavior and Evolution 15, 276–293.

Long CA (1982). Comparison of the Nest-Site Distraction Displays of Black-Capped Chickadee and White-Breasted Nuthatch. Wilson Bull. 94, 216–218.

Lorenz K (1970). On aggression (Harper & Row).

Lorenz K (1981). The foundations of ethology (Springer-Verlag).

Maynard Smith J (1979). Game Theory and the Evolution of Behaviour. Proc. Royal Soc. London Series B, Biol. Sci 205, 475–488.

Miczek KA, de Almeida RMM, Kravitz EA, Rissman EF, de Boer SF, and Raine A (2007). Neurobiology of escalated aggression and violence. J. Neurosci 27, 11803–11806. [PubMed: 17978016]

Morris D (1957). “Typical Intensity” and Its Relation to the Problem of Ritualisation. Behaviour 11, 1–12.

Moynihan M (1955). Types of Hostile Display. The Auk 72, 247–259.

Pfeiffer BD, Ngo TTB, Hibbard KL, Murphy C, Jenett A, Truman JW, and Rubin GM (2010). Refinement of Tools for Targeted Gene Expression in *Drosophila*. Genetics 186, 735–755. [PubMed: 20697123]

Ramdya P, Lichocki P, Cruchet S, Frisch L, Tse W, Floreano D, and Benton R (2014). Mechanosensory interactions drive collective behaviour in *Drosophila*. Nature 519, 233–236. [PubMed: 25533959]

Shine R (2008). Function and evolution of the frill of the frillneck lizard, *Chlamydosaurus kingii* (*Sauria: Agamidae*). Biol. J. Linnean Soc 40, 11–20.

Stokes AW (1962). Agonistic Behaviour among Blue Tits at a Winter Feeding Station. Behaviour 19, 118–138.

Tinbergen N (1950). The hierarchical organization of nervous mechanisms underlying instinctive behaviour In Physiological Mechanisms in Animal Behaviour (Academic Press, Inc). 305–312.

Tinbergen N (1954). The Origin and Evolution of Courtship and Threat Display In Evolution as a Process (Unwin Brothers Limited) Huxley J, Hardy AC and Fords EB (Eds). 233–249.

Tinbergen N (1963). On aims and methods of Ethology. Zeitschrift für Tierpsychologie 20, 410–433.

von Holst E, and von Saint Paul U (1962). Electrically Controlled Behavior. Sci. Am 206, 50–59. [PubMed: 13908550]

von Philipsborn AC, Liu T, Yu JY, Masser C, Bidaye SS, and Dickson BJ (2011). Neuronal Control of *Drosophila* Courtship Song. Neuron 69, 509–522. [PubMed: 21315261]

von Reyn CR, Breads P, Peek MY, Zheng GZ, Williamson WR, Yee AL, Leonardo A, and Card GM (2014). A spike-timing mechanism for action selection. Nat. Neuro 17, 962–970.

Wang L, and Anderson DJ (2010). Identification of an aggression-promoting pheromone and its receptor neurons in *Drosophila*. Nature 463, 227–231. [PubMed: 19966787]

Wang L, Chen IZ, and Lin D (2015). Collateral pathways from the ventromedial hypothalamus mediate defensive behaviors. Neuron 85, 1344–1358. [PubMed: 25754823]

Wang L, Dankert H, Perona P, and Anderson DJ (2008). A common genetic target for environmental and heritable influences on aggressiveness in *Drosophila*. PNAS 105, 5657–5663. [PubMed: 18408154]

Wang L, Han X, Mehren J, Hiroi M, Billeter JC, Miyamoto T, Amrein H, Levine JD, and Anderson DJ (2011). Hierarchical chemosensory regulation of male-male social interactions in *Drosophila*. Nat. Neuro 14, 757–762.

Watanabe K, Chiu H, Pfeiffer BD, Wong AM, Hoopfer ED, Rubin GM, and Anderson DJ (2017). A Circuit Node that Integrates Convergent Input from Neuromodulatory and Social Behavior-Promoting Neurons to Control Aggression in *Drosophila*. Neuron 95, 1112–1128. [PubMed: 28858617]

Whitman CO (1919). The behavior of pigeons. (Carnegie Institution).

Wu M, Nern A, Williamson WR, Morimoto MM, Reiser MB, Card GM, and Rubin GM (2016). Visual projection neurons in the *Drosophila* lobula link feature detection to distinct behavioral programs. eLife 5, e21022. [PubMed: 28029094]

Xu X, Coats JK, Yang CF, Wang A, Ahmed OM, Alvarado M, Izumi T, and Shah NM (2012). Modular Genetic Control of Sexually Dimorphic Behaviors. Cell 148, 596–607. [PubMed: 22304924]

Yamamoto D, and Koganezawa M (2013). Genes and circuits of courtship behaviour in *Drosophila* males. Nat. Rev. Neurosci 14, 681–692. [PubMed: 24052176]

Yamamoto D, Sato K, and Koganezawa M (2014). Neuroethology of male courtship in *Drosophila*: from the gene to behavior. J. Comp. Phys. A 200, 251–264.

Yang CF, and Shah NM (2014). Representing Sex in the Brain, One Module at a Time. Neuron 82, 261–278. [PubMed: 24742456]

Yang T, and Shah NM (2016). Molecular and neural control of sexually dimorphic social behaviors. Curr. Op. Neurobiol 38, 89–95. [PubMed: 27162162]

Yu JY, Kanai MI, Demir E, Jefferis GSXE, and Dickson BJ (2010). Cellular Organization of the Neural Circuit that Drives *Drosophila* Courtship Behavior. Curr. Biol 20, 1602–1614. [PubMed: 20832315]

Yurkovic A, Wang O, Basu AC, and Kravitz EA (2006). Learning and memory associated with aggression in *Drosophila melanogaster*. PNAS 103, 17519–17524. [PubMed: 17088536]

- Fly threat displays are comprised of multiple motor elements
- Modular AIP neurons control threat displays independently of other aggressive behaviors
- AIP neuron activation can mimic bimodal sensory cues and evoke variable motor output
- Threat displays promote, but are not required for, conspecific target repulsion

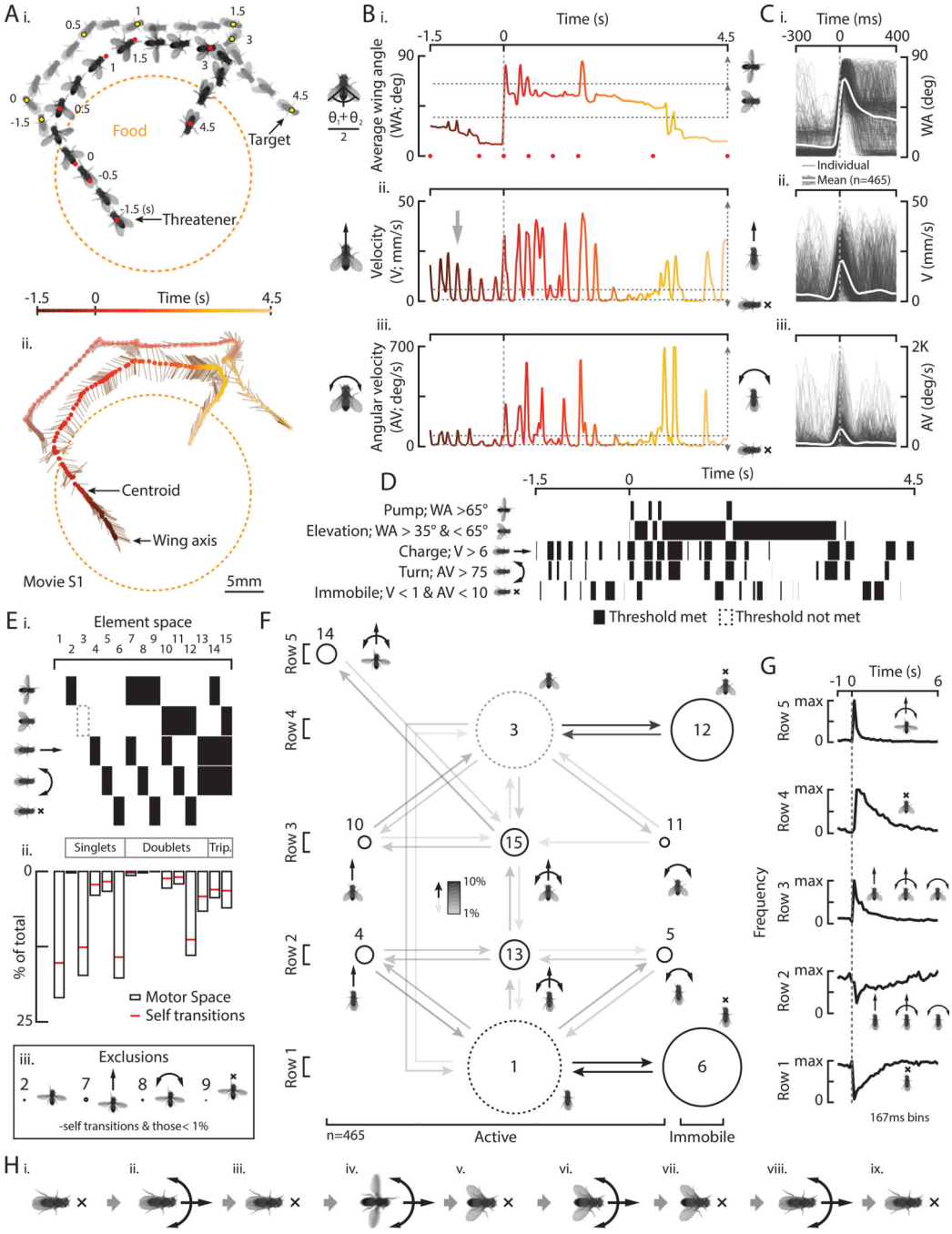

Figure 1: Natural threat displays are comprised of distinct motor elements.

A) Individual frames (i) and a resultant stick figure trajectory (ii) shows a threatener in relation to a target fly, food, and time. **B)** The average wing angle (WA, i), velocity (V, ii), and angular velocity (AV, iii) from A, color coded to time. **C)** WA (i), V (ii), and AV (iii) for 465 individual threats (light gray) and the mean (white). **D)** Binarization of five elements in B according to the thresholds indicated. **E)** Possible combinations in "element space" (i), an element space histogram of all threats (ii, bout +/− 0.5s), and exclusions (iii). **F)** A transition diagram for all threats. Node size represents relative proportions from Eii and arrow shading

represents relative non-self-transition percentage. **G)** The frequency of row specific elements in time. **H)** A typical threat sequence.

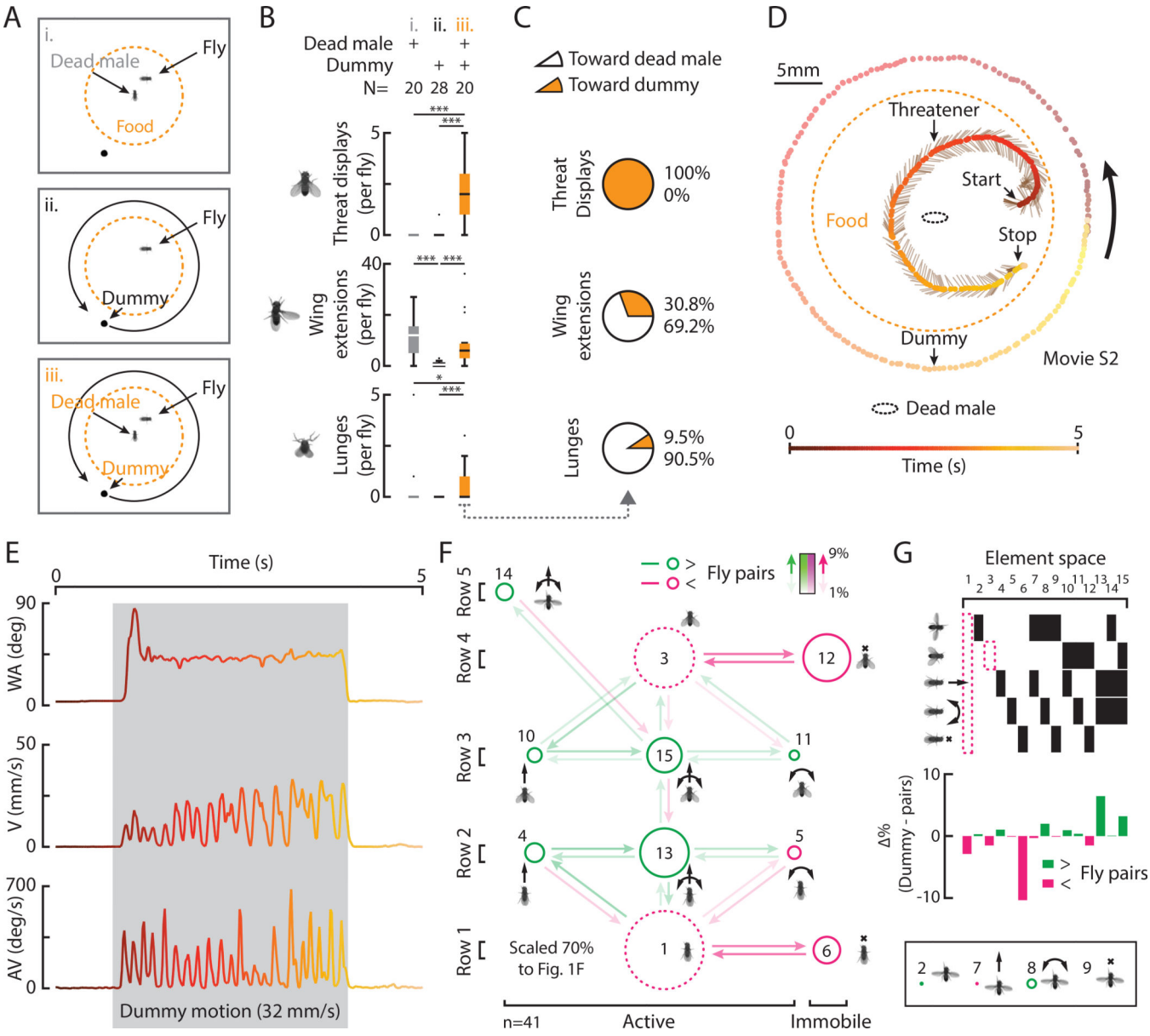

Figure 2: Chemosensory cues plus a moving object suffice to evoke threats.

A) Experimental conditions. **B)** Total behaviors per fly evoked in conditions indicated. (Pairwise and multiple comparison tests; *=p<0.05; **=p<0.01; ***=p<0.001 throughout) **C)** The percent of behaviors directed toward the dead male or the dummy in condition iii. **D)** A trajectory shows a threatener in relation to a dead male, a dummy, food, and time. **E)** WA, V, and AV from D, color coded to time. **F)** A transition diagram for all threats (condition iii, n=41). **G)** The relative differences in element space from threats by WT pairs (Fig. 1Eii) where green indicates increases and magenta, decreases.

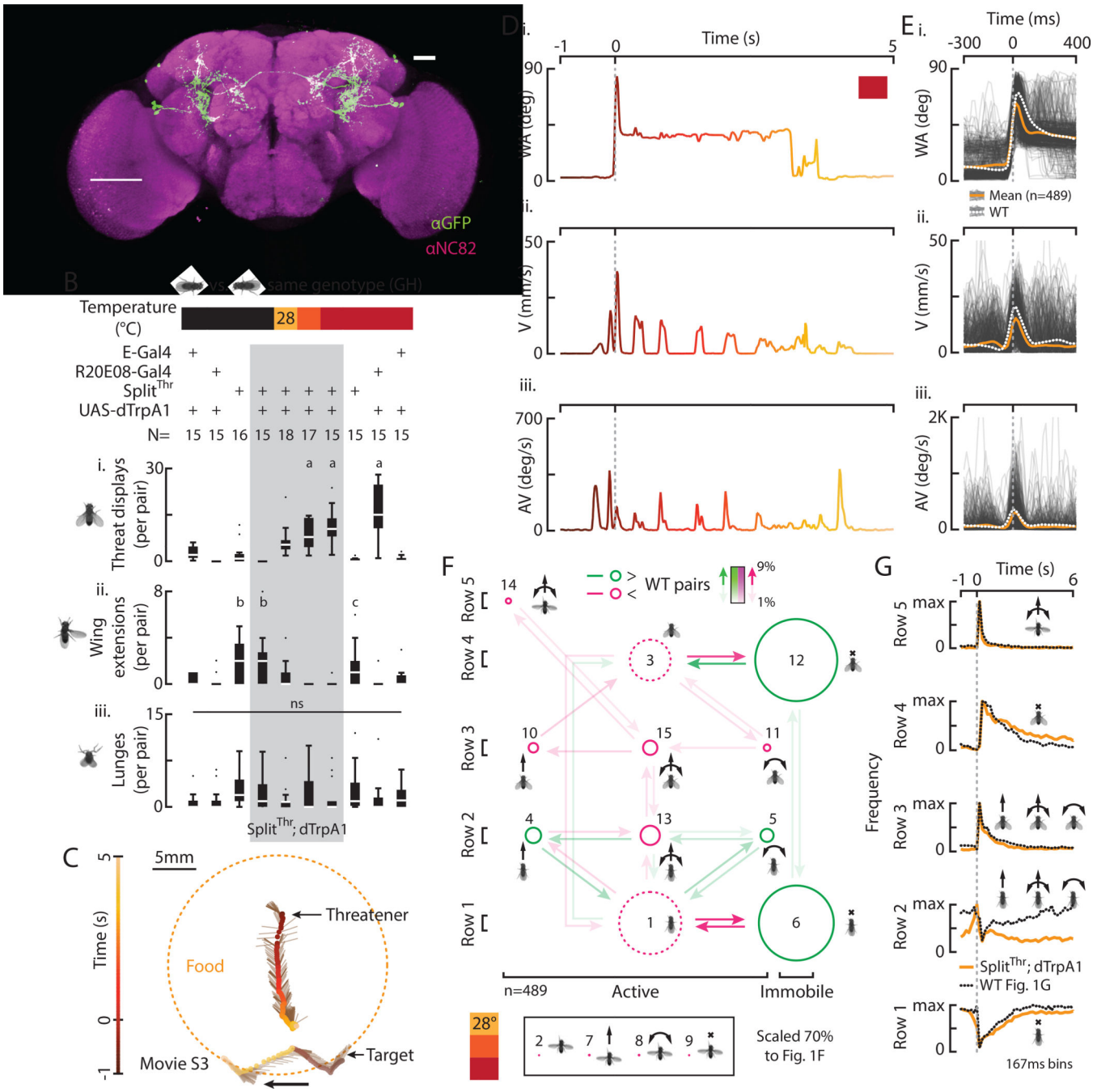

Figure 3: Identification of neurons that control threat displays.

A) A z-stack of Split^{Thr};GFP labeling two classes of neurons. Scale bar is 50μm. **B)** Total behaviors per pair (i-iii) according to genotype and temperature. **C)** A trajectory shows an induced threatener in relation to a target fly, food, and time. **D)** WA (i), V (ii), and AV (iii) from C, color coded to time. **E)** WA (i), V (ii), and AV (iii) for 489 threats (light gray) and the mean of induced (orange) and WT threats (dashed white). **F)** A transition diagram for induced threats (n=489). **G)** The frequency of row specific elements in time with WT data overlaid (dashed line).

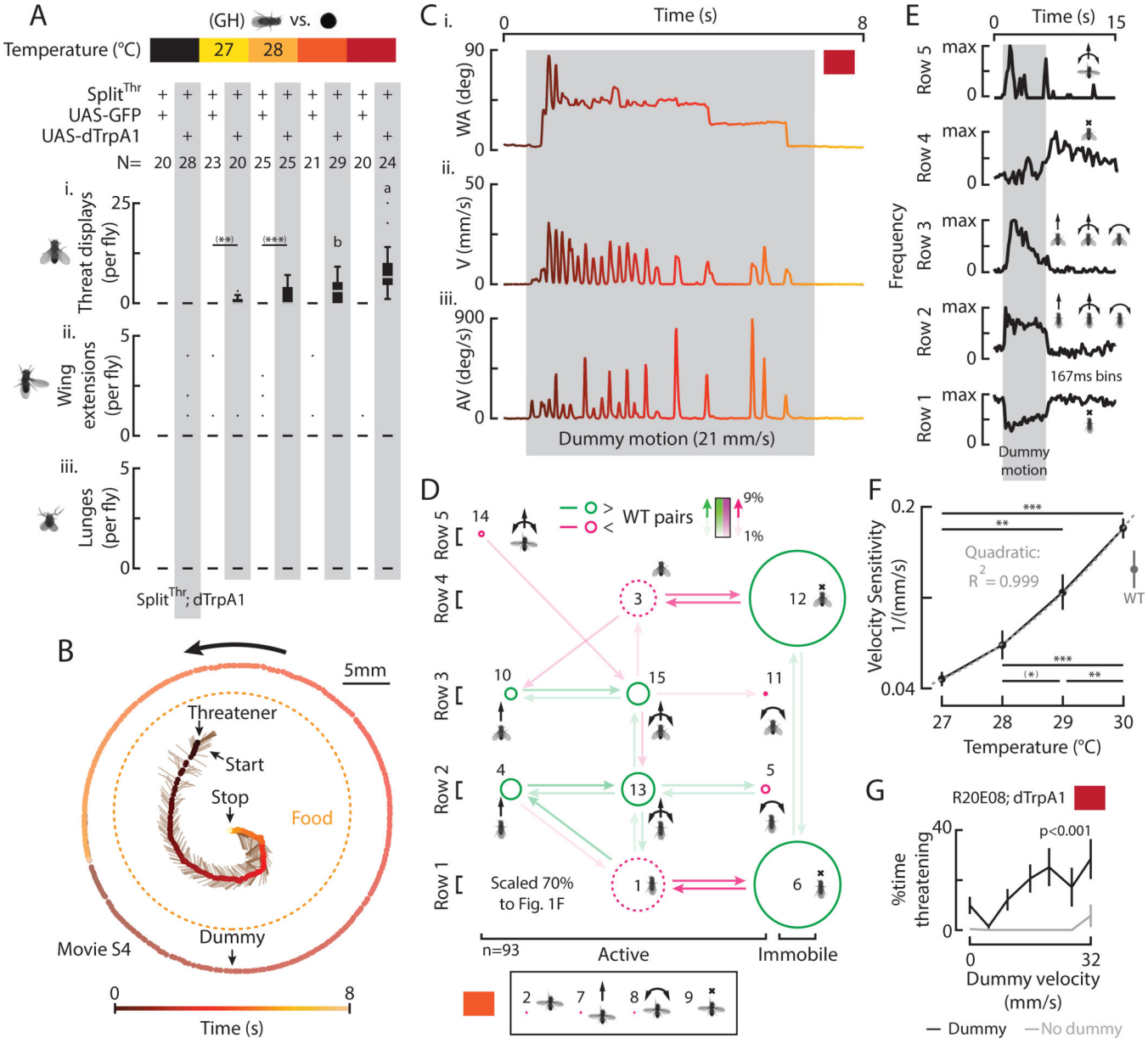

Figure 4: Thermogenetic activation of solitary Split^{Thr} flies substitutes for male cues and enhances sensitivity to dummy motion.

A) Total behaviors per fly (i-iii), according to genotype and temperature, in the presence of a moving dummy. ((*) indicates pairwise significance that did not survive multiple comparison tests throughout). **B)** A trajectory shows an induced threatener in relation to a moving dummy, food, and time. **C)** WA (i), V (ii), and AV (iii) for B, color coded to time. **D)** A transition diagram for all threats expressed in the presence of a dummy (n=93, 29°). **E)** The frequency of row specific elements in time, aligned to dummy motion (Fig. S5A, orange). **F)** Mean velocity sensitivity (1/ minimum dummy velocity evoking a threat ±SEM) vs. temperature with WT data from Fig. S2Biii. **G)** Mean percent of time ±SEM R20E08 activated flies expressed threats with (black) and without (gray) a dummy. (p-value from one-way ANOVA).

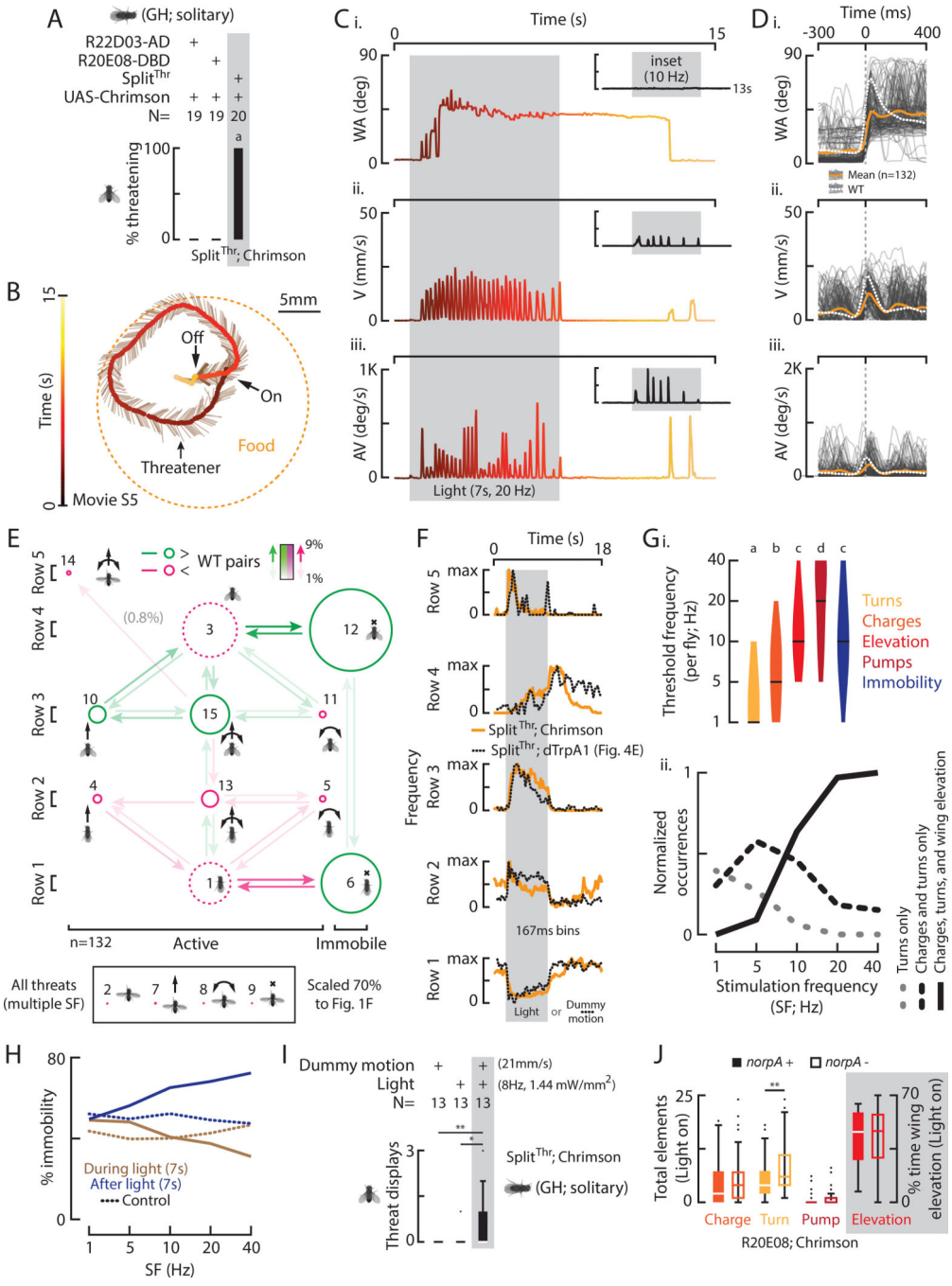

Figure 5: Optogenetic activation of Split^{Thr} neurons substitutes for sensory cues and induces different threat motor elements in a threshold-dependent manner.

A) Percent of flies with indicated genotypes that expressed at least one light induced threat. **B)** A trajectory shows an induced threatener in relation to food and time. **C)** WA (i), V (ii), and AV (iii) for B, color coded to time with other data inset (Fig. S6B). **D)** WA (i), V (ii), and AV (iii) for 132 threats (light gray) and the mean of induced (orange) and WT threats (dashed white). **E)** A transition diagram for induced threats. **F)** The frequency of row specific elements in time with data from Fig. 4E overlaid (dashed line, different time scale).

G) Violin plots (with median) of the per fly threshold stimulation frequency (I, SF) required to elicit the indicated motor elements and (ii) the normalized occurrences of trials with the most prevalent elements and combinations (Fig. S6Iii) according to SF. **H)** Percent immobility during or after light vs. SF. **I)** Total threats induced by dummy motion, low frequency light, and both in combination with stimulus intensities indicated. **J)** Total elements expressed by R20E08 activated flies with *norpA*+ (solid bars) or *norpA*- (open bars).

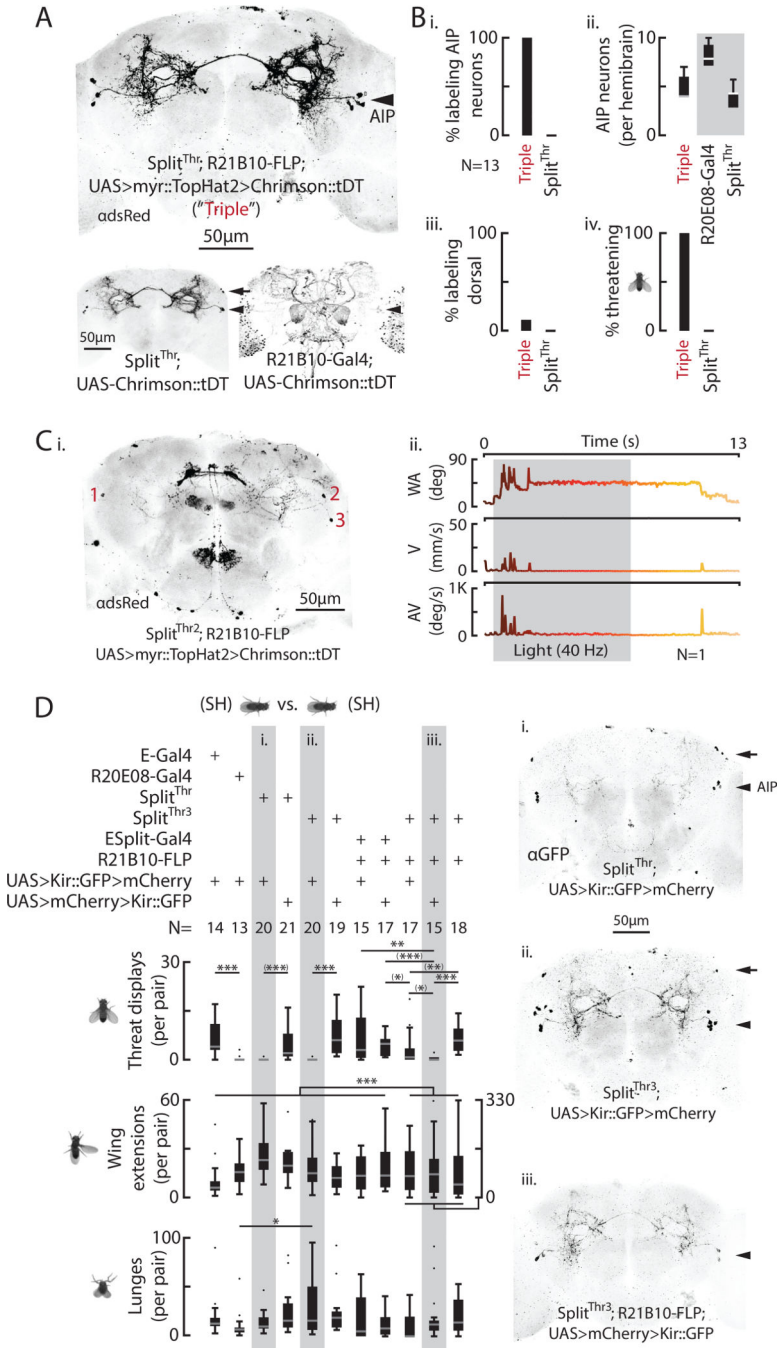

Figure 6: AIP neurons are sufficient and necessary for natural threat displays.

A) Representative Chrimson::tDT expression from a "triple" intersection (top) between Split^{Thr} (bottom left) and R21B10 (Gal4, bottom right) with AIP (arrowheads) and dorsal neurons (arrows) indicated. **B)** This intersection labels AIP neurons (i, ii), not (mostly) dorsal neurons (iii), and promotes light induced threats (iv). Grey box (ii) indicates UAS-Chrimson not FLP-ON. **C)** Chrimson::tDT expression (i) in 3 AIP neurons in a fly that exhibited a light induced, multi element threat (ii; Split^{Thr2}). **D)** Total behaviors per pair (left) according to genotype. (Significance from pairwise and multiple comparisons tests as

indicated). Representative brain expression (right) for Split^{Thr} (i), Split^{Thr3} (ii), and a triple intersection (iii) with AIP (arrowheads) and dorsal neurons (arrows) indicated. Scale bars (A, C, D) are 50μm.

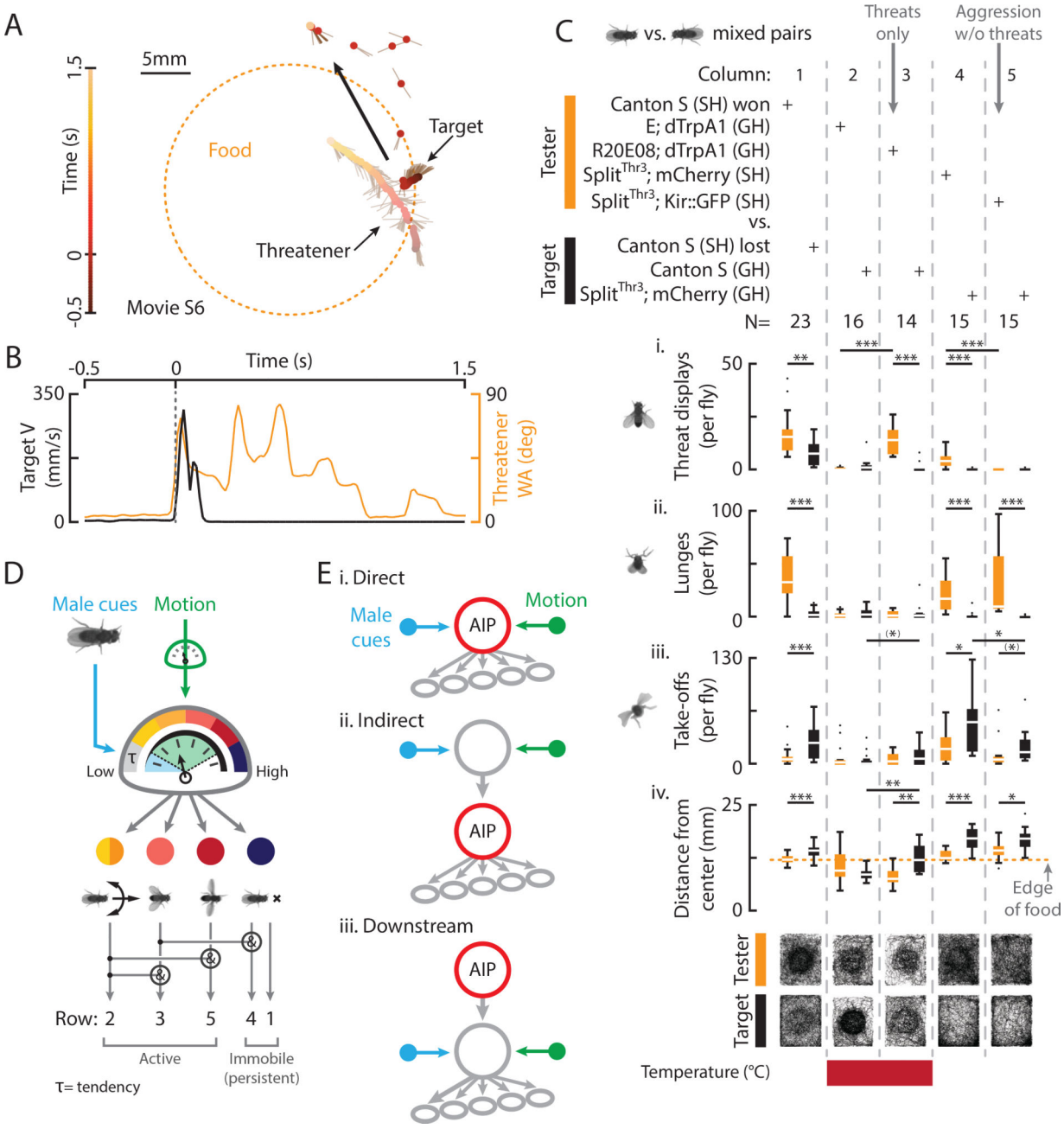

Figure 7: Threats function to repel opponents and are mediated by a scalable brain module.

A) A trajectory shows a target fly taking off in relation to a threatener, food, and time. **B)** Target V (black) and threatener WA (orange) for A. **C)** Total behaviors (i-iii) and distance from the center of the food (iv) per fly for mixed pairs of the indicated genotypes (bottom = transit histograms for all flies). **D)** Threats are evoked by male cues and visual motion, mediated by modular AIP neurons, and comprised of threshold-dependent motor elements. **E)** Conceivable circuit diagrams for the interaction of sensory input, AIP neurons, and motor output (not mutually exclusive).

KEY RESOURCES TABLE

REAGENT or RESOURCE	SOURCE	IDENTIFIER
Antibodies		
anti-DsRed (rabbit)	Clontech	Cat#632496 RRID:AB_10013483
nc82 (mouse)	Developmental Studies Hybridoma Bank	RRID:A2314866
anti-GFP (mouse)	Thermo Fisher Scientific	Cat#A11120 RRID:AB_221568
anti-GFP (rabbit)	Thermo Fisher Scientific	Cat#A11122 RRID:AB_221569
Goat anti-mouse Alexa Flour 488	Thermo Fisher Scientific	Cat#A11001 RRID:AB_2534069
Goat anti-rabbit Alexa Flour 488	Thermo Fisher Scientific	Cat#A11008 RRID:AB_143165
Goat anti-rabbit Alexa Flour 568	Thermo Fisher Scientific	Cat#A11011 RRID:AB_143157
Goat anti-mouse Alexa Flour 633	Thermo Fisher Scientific	Cat#A21050 RRID:AB_141431
Rabbit anti-FruM	Barry Dickson	N/A
Rat anti N-cadherin	Developmental Studies Hybridoma Bank	RRID:AB221568
Chemicals, Peptides, and Recombinant Proteins		
All *trans*-Retinal	Sigma-Aldrich	Cat#R2500
Insect-A-Slip	BioQuip Products	Cat#2871B
Experimental Models: Organisms/Strains		
Drosophila: Wild-type CantonS	M. Heisenberg	N/A
Drosophila: Quad olfactory mutant *IR8a, IR25a, OR83b, Gr63a*	Ana Silbering, Richard Benton	N/A
Drosophila: R20E08-Gal4 (attp2)	Rubin lab	RRID:BDSC_69771
Drosophila: pBDP-Gal4U “empty” (attp2)	Rubin lab	N/A
Drosophila: Otd-nls::FLPo (attp40)	K. Watanabe	N/A
Drosophila: 20×UAS>tdTomato>dTrpA1 (VK5)	Rubin lab	N/A
Drosophila: 20×UAS>dTrpA1>tdTomato (VK5)	Rubin lab	N/A
Drosophila: 10×UAS >mCherry>Kir 2.1::GFP (attp2)	K. Watanabe	N/A
Drosophila: 10× UAS>Kir 2.1::GFP>mCherry (attp2)	K. Watanabe	N/A
Drosophila: 10×UAS-IVS-myr::GFP (attp5)	Rubin lab	N/A
Drosophila: R22D03-AD (attp40)	Rubin lab	N/A
Drosophila: R20E08-DBD (attp2)	Rubin lab	N/A
Drosophila: UAS-dTrpA1	P. Garrity	N/A
Drosophila: 20×UAS-IVS-Syn21-Chrimson::tdT-3.1 (VK5)	Rubin lab (this study)	N/A
Drosophila: norpA^{36}	Bloomington *Drosophila* Stock Center	9048 RRID:BDSC_9048
Drosophila: R21B10-Gal4 (attp2)	Rubin lab	RRID: BDSC_49295
Drosophila: R21B10-FLP	H. Inagaki	N/A

REAGENT or RESOURCE	SOURCE	IDENTIFIER
Drosophila: 20×UAS-FRT> myr::TopHat2->FRT-Syn21-Chrimson::tdT 3.1 (VK5)	Rubin lab (this study)	N/A
Drosophila: R20E08-AD (attp40)	Rubin lab	N/A
Drosophila: R34H05-DBD (attp2)	Rubin lab	N/A
Drosophila: R22D03-DBD (attp2)	Rubin lab	N/A
Drosophila: pBDP-AD “empty” (attp2)	Rubin lab	N/A
Drosophila: pBDP-DBD “empty” (attp2)	Rubin lab	N/A
Drosophila: 10×UAS-DenMark (attp40)	Rubin lab	N/A
Drosophila: 3×UAS-IVS-syt-GFP (attp18)	Rubin lab	N/A
Drosophila: 20E08-LexA (attp40)	Rubin lab	N/A
Drosophila: 13×LexAOP-GFP (attp8)	Rubin lab	N/A
Drosophila: R11F03-DBD (attp2); R71D08-AD (VK27)	Y. Aso, Rubin lab	N/A
Drosophila: 10×UAS-tdT (attp18)	Rubin lab	N/A
Software and Algorithms		
Bias video acquisition	Will Dickson, IORodeo	N/A
Caltech Fly Tracker	Eyrun Eyjolfsdottir and Pietro Perona	N/A
Janelia Automatic Animal Behavior Annotator (JAABA)	Kristen Branson, Janelia Research Campus	N/A
Matlab R2013b	Mathworks	RRID: SCR_001622
Fiji	https://fiji.sc/	RRID: SCR_002285